Title
Physics-Based Hazard Assessment for Critical Structures Near Large Earthquake Sources

Journal
Pure and Applied Geophysics, 174(9)

ISSN
0033-4553

Authors
Hutchings, L
Mert, A
Fahjan, Y
et al.

Publication Date
2017-09-01

DOI
10.1007/s00024-017-1572-4

Peer reviewed

Physics-Based Hazard Assessment for Critical Structures Near Large Earthquake Sources

- Authors
- Authors and affiliations

- L. Hutchings
- A. Mert
- Y. Fahjan
- T. Novikova
- A. Golara
- M. Miah
- E. Fergany
- W. Foxall

Abstract

We argue that for critical structures near large earthquake sources: (1) the ergodic assumption, recent history, and simplified descriptions of the hazard are not appropriate to rely on for earthquake ground motion prediction and can lead to a mis-estimation of the hazard and risk to structures; (2) a physics-based approach can address these issues; (3) a physics-based source model must be provided to generate realistic phasing effects from finite rupture and model near-source ground motion correctly; (4) wave propagations and site response should be site specific; (5) a much wider search of possible sources of ground motion can be achieved computationally with a physics-based approach; (6) unless one utilizes a physics-based approach, the hazard and risk to structures has unknown uncertainties; (7) uncertainties can be reduced with a physics-based approach, but not with an ergodic approach; (8) computational power and computer codes have advanced to the point that risk to structures can be calculated directly from source and site-specific ground motions. Spanning the variability of potential ground motion in a predictive situation is especially difficult for near-source areas, but that is the distance at which the hazard is the greatest. The basis of a “physical-based” approach is ground-motion syntheses derived from physics and an understanding of the earthquake process. This is an overview paper and results from previous studies are used to make the case for these conclusions. Our premise is that

50 years of strong motion records is insufficient to capture all possible ranges of site and propagation path conditions, rupture processes, and spatial geometric relationships between source and site. Predicting future earthquake scenarios is necessary; models that have little or no physical basis but have been tested and adjusted to fit available observations can only “predict” what happened in the past, which should be considered description as opposed to prediction. We have developed a methodology for synthesizing physics-based broadband ground motion that incorporates the effects of realistic earthquake rupture along specific faults and the actual geology between the source and site.

Keywords

PSHA ergodic assumption physics based earthquake hazard empirical Green’s functions

1 Introduction

It is estimated that, worldwide, 20% of nuclear reactors are operating in areas of significant seismic activity. Nuclear facilities are designed so that earthquakes and other external events will not jeopardize the safety of the plant. The International Atomic Energy Agency (IAEA) has a Safety Guide on Seismic Risks for Nuclear Power Plants. Various systems are used in planning, including Probabilistic Seismic Hazard Assessment (PSHA), which is recommended by IAEA and widely accepted. Another way regulators prepare for the safety of nuclear reactors is requiring reactors to withstand a “design basis” M_w 6.7 earthquake directly beneath the reactor.

Reliable estimates of ground motions for engineered structures depend on accurate estimates of the source location of potential earthquakes, their rupture characteristics, and wave propagation and site response effects. We are concerned with the near-source area, where the ground motion hazard is most variable and the highest. We argue that attempts to simplify calculations of ground motion as well as the reliance on history and the ergodic assumption have put critical structures at risk. Current PSHA studies are based upon the ergodic assumption that the randomness in space from several sources is the same as the randomness in time from the same source (Anderson and Brune 2000). Four nuclear reactors have experienced earthquakes that exceed their design ground motion due to unexpectedly large nearby earthquakes. The Humboldt Bay nuclear reactor, California had peak ground accelerations of 392 g (although the operator at the time claimed these values were unreliable) against design criteria of 200 g from the M_w 6.9, 1980 Eureka earthquake 30 km away (USNRC 1980). It also experienced similar level shaking from the M_w 5.6, 1975 Ferndale earthquake 32 km away (USNRC 1980, appendix A6). The North Anna, Virginia nuclear reactor had peak ground acceleration of 255 Gal, against

design basis of 176 Gal from the M_w 5.8, Virgina 2011 earthquake with epicenter 20 km away (Wollen et al. 2012). All three of these earthquakes occurred on previously unidentified faults. The Kashiwazaki–Kariwa nuclear reactor, Japan had peak ground accelerations of 332–680 Gal at two reactors against design ground motions of 450 Gal from the M_w 6.6, 2007 Chuetsu–Oki earthquake 23 km from the facility. This earthquake occurred on a previously identified fault, but the potential effect of an earthquake was underestimated (IAEA 2007). Empirical relations were used to predict the ground motions. A Nuclear and Industrial Safety Agency (NISA 2008) identified local geological factors affecting wave propagation and response in addition to an unexpected rupture process as contributing to a magnification of the seismic intensity at the plant. The Fukushima nuclear power plant experienced catastrophic failure from a tsunami, but the design ground motion was also exceeded for both Fukushima nuclear reactors plants from the 2011 M_w 9.0, Tohoku earthquake. Design criteria had been upgraded in 2008, and was at horizontal 441–489 Gal for Daiichi and 415–434 Gal for Daini at the time of the earthquake. The interim recorded data for both plants show that 550 Gal was the maximum for Daiichi, in the foundation of unit 2 and 254 Gal was maximum for Daini units 2, 3, and 5, which exceeded their maximum response acceleration design basis in the E–W direction by about 20% (IAEA 2014). Significant ground motion continued over 130–150 s, much longer than design criteria. High ground motions from these earthquakes occurred unexpectedly due to a failure to clearly identify the earthquake source, rupture characteristics, wave propagation, and site response effects. All these ground motions discussed above could have been anticipated, in part, with a physics-based estimation instead of an estimation based on history or a regression on previous data.

Modeling the rupture process of earthquakes is important to modeling near-source ground motion as is local parameters such as geology, fault-station geometry, propagation path, and site response. These can all have significant variations throughout the world. Many researchers have simplified the source to be a point with a magnitude (Abrahamson and Bommer 2009; and several others). Following this, the source has been defined by regression on past earthquakes to provide spectral shapes (Boore et al. 1997), or even to use moderate earthquakes as Green's functions that are scaled to match larger earthquakes' spectra through scaling relations (Irikura 1986). Recently, finite rupture has been included in PSHA by summing point source random vibration seismograms for high frequencies (Atkinson and Macias 2009; Graves and Pitarka 2010). Random vibrations cannot add coherently to replicate phasing effects that cause buildup of large-amplitude high-frequency arrivals that are particularly hazardous to structures. For some applications, the source has been removed entirely and "appropriate" seismograms have been used to predict the effect of

structures. All these approaches are based upon fitting data to earthquakes that have occurred in the past, or upon unrealistic earthquake models.

Wave propagation and site response have also been difficult to quantize. Several studies have used finite-difference modeling to account for low-frequency wave propagation, and this has proven effective because it is not necessary to thoroughly understand the regional geology to model long-period wave propagation. However, for frequencies higher than 1 Hz, geologic heterogeneity has a significant effect on the resulting predicted ground motion. Few, if any, studies have validated ground motion propagation Green's functions at frequencies above 1 Hz, though the significant frequency band for nuclear reactors can be as high as 50 Hz.

With the ergodic assumption, correlation between the ground motion and the specific source, path, and site is lost, thereby leading to potentially higher total uncertainty in hazard estimates than if each release of energy at an earthquake source was individually propagated to the site of interest. Even if the source is moved beneath the site to account for unknown faults, a physics-based calculation of the ground motion is necessary. The next-generation attenuation (NGA) project has utilized physics-based source modeling for near-source effects. This has been used for general cases and to fill in the empirical database of ground motion parameters to improve ground motion prediction equations (GMPE's). This is a form of the ergodic assumption as it assumes that few idealized cases can be extended to specific sites.

We suggest that for critical structures near large earthquake sources: (1) the ergodic assumption, recent history, and simplified descriptions of the hazard are not appropriate to rely on for earthquake ground motion prediction and can lead to a mis-estimation of the hazard and risk to structures; (2) a physics-based approach can address these issues; (3) a physics-based source model must be provided to generate constructive and destructive phasing effects from finite rupture due to a particular source-station geometry; (4) wave propagations and site response should be site specific; (5) a much wider search of possible sources of ground motion can be achieved computationally with a physics-based approach; (6) unless one utilizes a physics-based approach, the hazard and risk to structures have unknown uncertainties; (7) uncertainties can be reduced with a physics-based approach, but not with an ergodic approach; (8) computational power and computer codes have advanced to the point that risk to structures can be calculated directly from source and site-specific ground motions. The basis of a "physical-based" approach is ground-motion syntheses derived from physics and an understanding of the earthquake process. We outline our methodology for synthesizing physics-based broadband ground motion that incorporates the effects of realistic earthquake rupture along specific faults and the actual geology between the source and site, and

implementation into PSHA. This is an overview paper and results from previous studies are used to make the case for these conclusions.

2 PSHA

Over the past fifty years the state-of-the-art practice for probabilistic seismic hazard analysis (PSHA) has been based on estimating the annual frequency of exceedance (or its reciprocal, return period) for a ground motion parameter at sites (i.e., a hazard curve, Cornell 1968). Typically, the parameter is peak acceleration or spectral response. It requires (1) an interpretation of seismic sources that constitute a hazard to a particular site so that the distances of earthquakes from the site can be determined; (2) an interpretation of earthquake recurrence for each source; (3) models of ground-motion prediction in the form of empirical attenuation relationships; (4) given these input evaluations, integration over all values of the variables to produce a hazard curve. The hazard curve incorporates the uncertainties in elements (1), (2), and (3) above. This is discussed further in SSHAC (1997). Risk to structures is then calculated by relating the level of the parameter estimated for annual frequency of exceedance to risk through empirical relations (Wang 2006; Conte et al. 2003) or to select a time history to calculate risk (Porter 2003; Baker and Cornell 2004).

Our physical-based PSHA (pb-PSHA) has the same elements of standard PSHA and risk analysis, but replaces element (3) with calculations of physical-based synthetic seismograms, and risk analysis with directly calculating the risk to structures from these seismograms. It is source and site specific; therefore, ground motions at a particular site include geometric relationships to sources and results will incorporate the finite faulting effects. If empirical Green's functions (EGFs) are also used, then actual propagation path and site effects will be included in the results. Furthermore, it relies on physical parameters to model sources. Because input parameters are correlated through a physical model, unrealistic combinations are excluded. This will naturally define the shape at the tails of distribution curves and truncate distributions of ground motions, thereby limiting "extreme" ground motions. It replaces the aleatory uncertainty that current PSHA studies estimate by regression of empirical parameters with epistemic uncertainty that is expressed by the variability in the physical parameters of the earthquake rupture process. A future area of research will be to identify significant parameters and determine their ranges. Source rupture parameters are not well known in most regions and the distribution of parameters must reflect the parameters' uncertainty based on physical arguments.

Current approaches to element (3) utilize historical recordings of earthquakes to develop "attenuation relations" that describe a parameter as

a function of earthquake magnitude, distance, and occasionally additional factors. These empirical data are forced to fit log-normal distributions with zero mean and standard deviation. This is shown in Fig. 1, where the tails of the distribution effectively go to infinity. The true shape of the distribution is unknown and contributes to errors in calculating the hazard. In estimating the hazard for the Yucca Mt. Repository, the design criterion was for peak acceleration with a probability of exceedance of 1×10^{-8}/year (five standard deviations), which resulted in a ground motion of 11 g (Stepp and Wong 2003). Andrews et al. (2007) attempted to limit the highest peak acceleration on physical grounds, effectively truncating the distribution.

Open image in new window

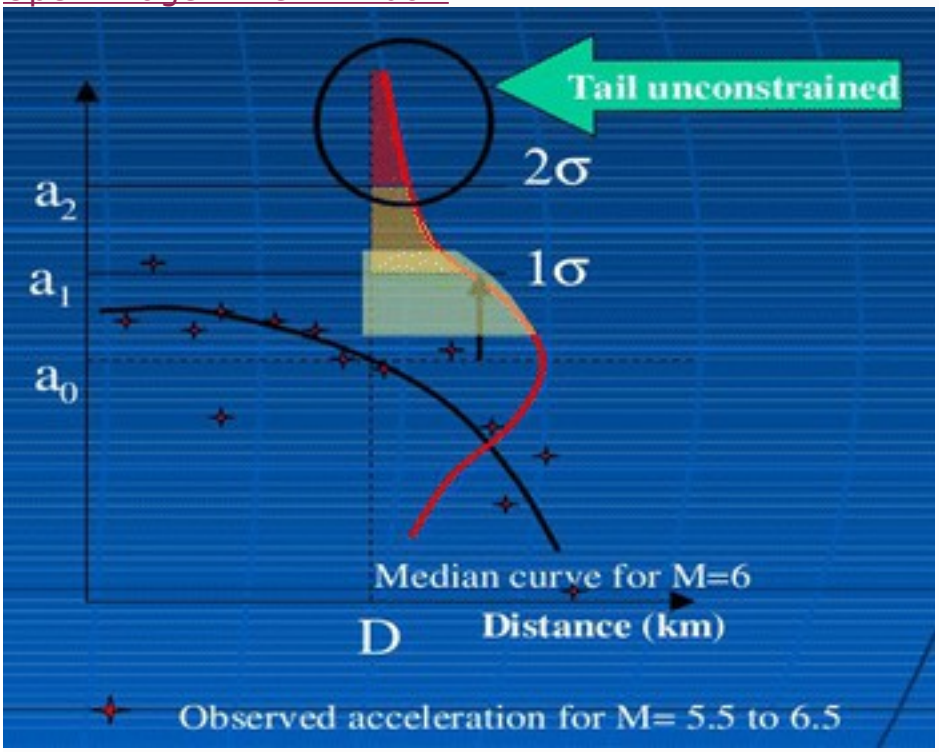

Fig. 1
A cartoon showing a normal distribution fit to data. The shape of the distribution is largely unconstrained by data primarily near the mean and the tails have no limit to predicted values of the parameter

To fully capture the uncertainties in hazard and risk analyses, all elements within the overall framework have to account for uncertain and incomplete data, inexact models of the phenomena, and intrinsic variability in the physical system being modeled. Uncertainty can be aleatory, which is due to inherent randomness of the process that cannot be modeled, or epistemic, which is due to uncertainty in knowledge about the processes. Epistemic uncertainty can be reduced by research; aleatory uncertainty is inherent in the system or process and thus cannot be reduced. These epistemic uncertainties and aleatory variability are always present, and capturing them fully is one of the major challenges in hazard and risk analysis.

Empirical attenuation relations have been shown to have uncertainty that has not been reduced over the past several decades of adding empirical recordings to regression relations (Bommer and Abrahamson 2006; Strasser et al. 2009). A physical-based approach offers a means to reduce uncertainty because it is primarily subject to epistemic uncertainty, whereas the regression approach is primarily subject to aleatory uncertainty.

For risk assessment, the reverse of developing attenuation relationships is typically used. This means that peak acceleration (or response spectra) is identified along with the controlling magnitude, distance, and geology, and then the empirical strong motion database is searched to find records that fit the desired parameters. These records may have very little in common with the actual ground motion that will occur at the site and the risk may, therefore, be miscalculated.

3 Examples

An example of what may contribute to the inability to reduce uncertainty in peak acceleration attenuation relations is shown by data from the 2006 M_w 6.0, Parkfield earthquake. Figure 2a shows recorded acceleration as a single value (peak acceleration) and the source as magnitude and distance from the fault compared to recent relations developed to predict such data (Abrahamson and Bommer 2009). At distances less than 10 km, the values are random and vary by a factor of 10 (more if the one value at 2 g is included). It is quite apparent that the data from 1–10 km is not represented by a log-normal distribution, but instead possibly a bi-modal boxcar distribution. Figure 2b shows a solution for the slip distribution of the earthquake obtained from inversion studies that presents why this may occur (Liu et al. 2006). Large-amplitude slip is randomly distributed throughout the fault and is separated by up to 30 km of distance. The amplitude of ground motion from such asperities is also randomly distributed. The variability of the source process has a randomizing effect when used to characterize earthquakes with simple relationships. The fault length is approximately 40 km and there is no way to know what location along the fault was the source of a recorded peak value. These values are likely different for each station. So, the idea of plotting a parameter as a function of distance from the fault probably only makes sense when stations are far enough away from the fault that the area of the fault does not contribute significantly to the distance calculation. Generally, these are distances from the fault where strong ground motions are not an issue anyway.

Open image in new window

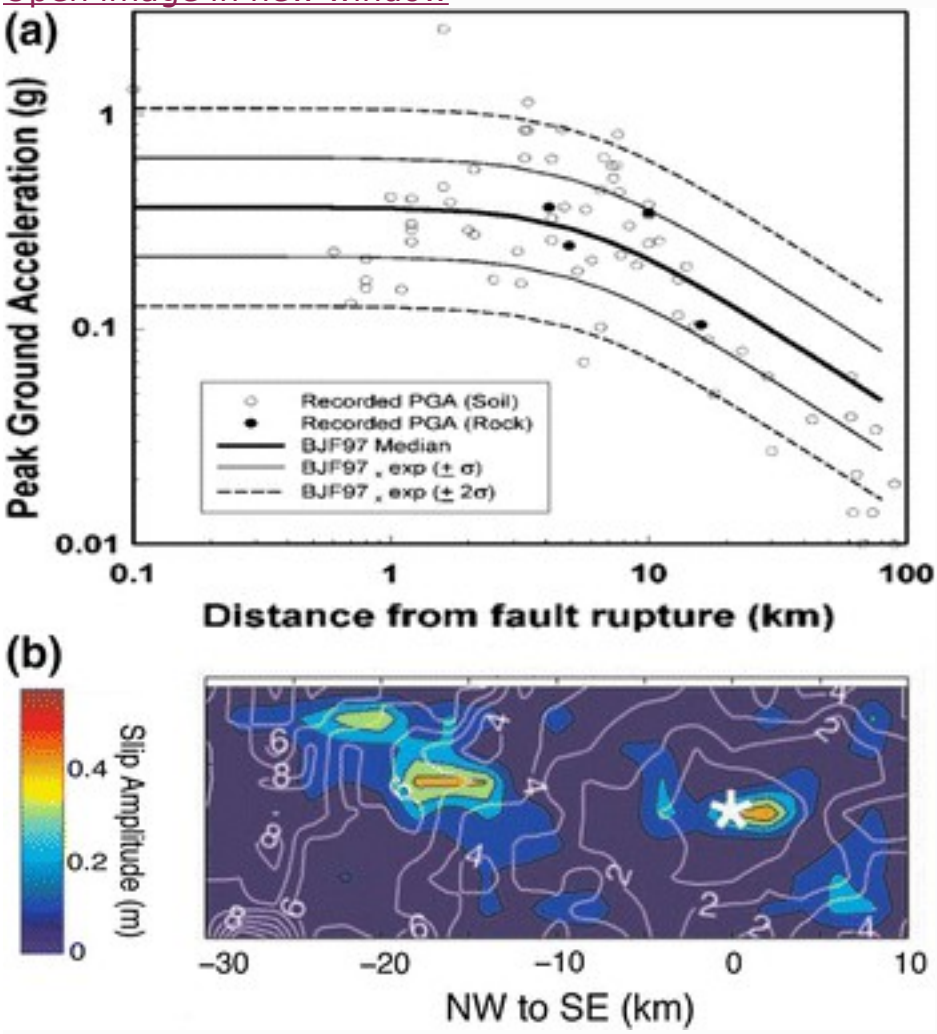

Fig. 2
2012 Parkfield earthquake. **a** Peak accelerations recorded and plotted as distance from the fault (Abrahamson and Bommer 2009), **b** one interpretation of the fault rupture displacement, with hotter colors being higher displacement, and possible asperities (Liu et al. 2006)

An example that suggests that asperities along a fault can be the source of peak acceleration is shown in Fig. 3. The ground motion with the highest peak recorded at the Kashiwazaki–Kariwa Nuclear Power complex (K–KNPP) from the previously mentioned M_w 6.6, 2007 Chuetsu–Oki earthquake arrived 5 s after the initial arriving S-wave energy, which was possibly ground motion caused by a late-occurring asperity some distance from the initial rupture of the earthquakes. Figure 3 shows three asperities identified by their considered contribution to the late-arriving energy.

Open image in new window

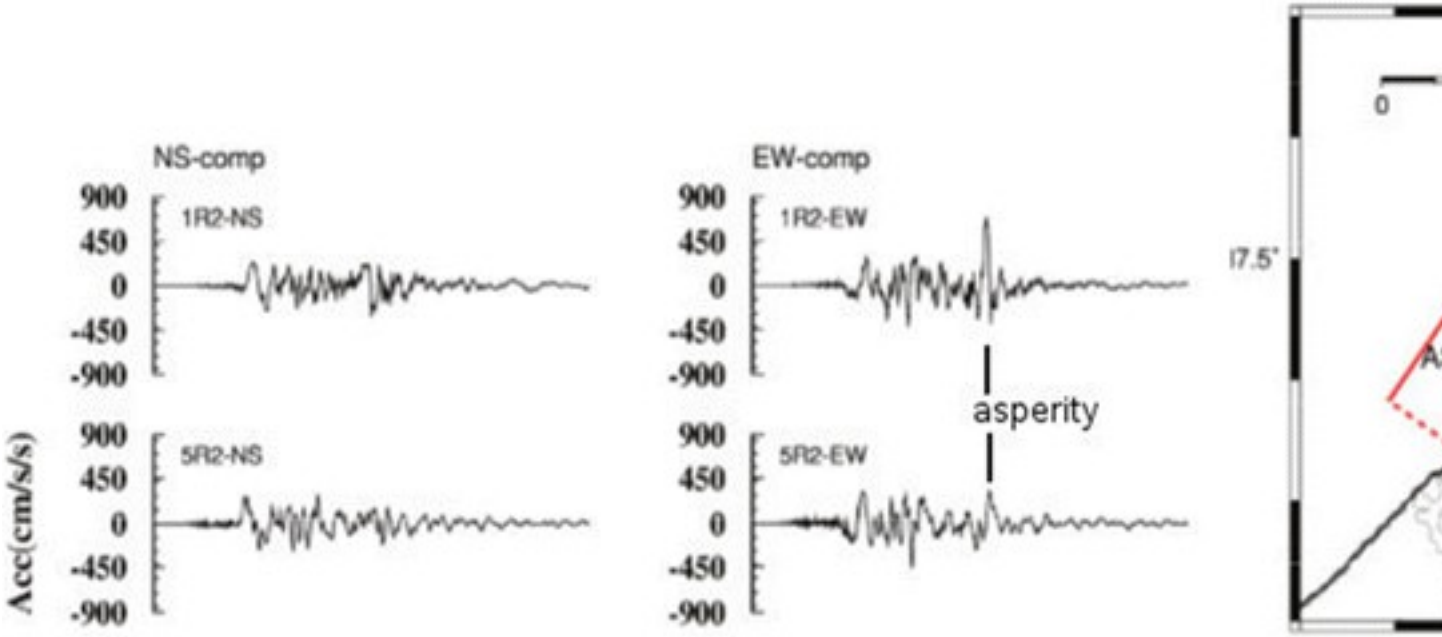

Fig. 3
a Ground motion at the K–KNPP complex from the 2007 earthquake at unit 1R2 (*top*) and 5R2 (*bottom*), from Uetake et al. (2008). Late-arriving large-amplitude phase on the E–W component may be from an asperity

Figure 4 shows the 1989 M_w 6.9, Loma Prieta earthquake recorded at two soil sites 67 and 68 km from the source. The difference in the peak acceleration and response spectra is up to a factor of eight. These are inter-earthquake differences; when intra-earthquake differences are considered the total variability is much greater. With this type of randomness in the earthquake process, it should not be a surprise that attempts to characterize earthquakes by simple regression approaches have not decreased uncertainty. We argue that the sample of earthquakes in the empirical database is insufficient to give an indication of the geometry, geology, rupture heterogeneities, and rupture processes of possible future earthquakes. Parallel to this is the need to accurately include the propagation and site response in ground motion simulations. Simple solutions such as distance used in GMPE's, random vibration or synthetic seismograms with simple source and geologic models are insufficient to characterize the complexities of the geology and its effects on high-frequency (>1 Hz) wave propagation.

Open image in new window

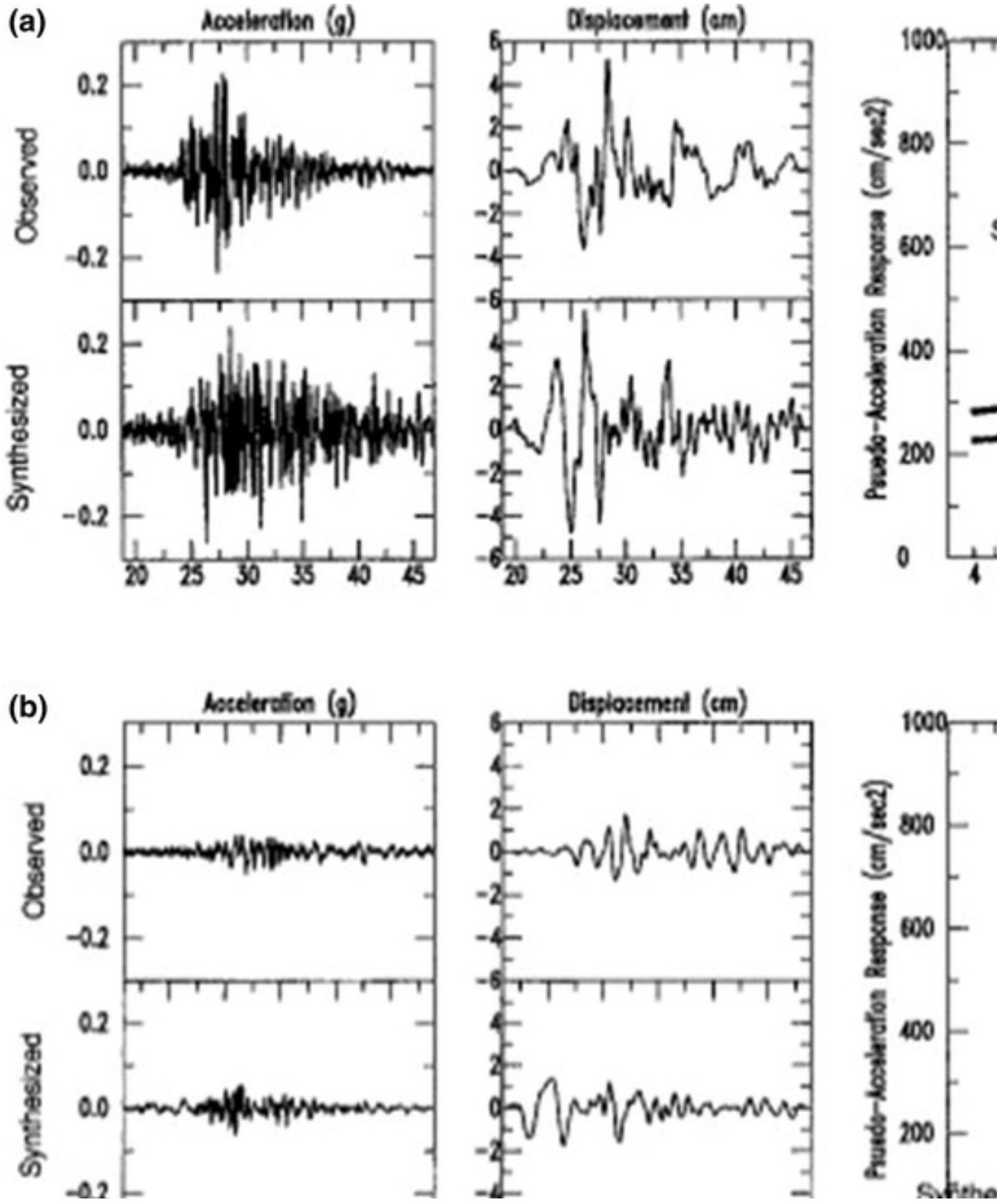
(a)
Acceleration (g)
Displacement (cm)
Observed
Synthesized
0.2
0.0
-0.2
6
4
2
0
-2
-4
-6
20
25
30
35
40
45
1000
800
600
400
200
0
Pseudo-Acceleration Response (cm/sec2)
(b)
Acceleration (g)
Displacement (cm)
Observed
Synthesized
Pseudo-Acceleration Response (cm/sec2)

Fig. 4
Records at soil sites 67 and 68 km from the Loma Prieta earthquake. *Left* observed and synthesized acceleration and displacement for one component (Jarpe and Kasameyer 1996). *Right* observed and synthesized AAR at the two sites (Jarpe and Kasameyer 1996) and the ±std for response spectra predicted from Boore et al. (1997)
Other examples of the randomness and variability in near-source ground motion and the likely inability of empirical relations to predict this motion are recorded response spectral values from the M_w 7.8, 1999 Chichi, Taiwan earthquake. Figure 5a shows locations near the fault (in red) where response spectra were calculated, all at approximately the same distance away. Figure 5b shows the distribution of response spectra calculated. This shows a factor of about 4 variations, which is notably better than the peak acceleration. This is likely due to the use of the entire seismogram rather than one value. So, response spectra may offer an approach to reduce uncertainty, but as discussed below, they are still not source or site specific and cannot provide the time series that may occur at a particular site.
Open image in new window

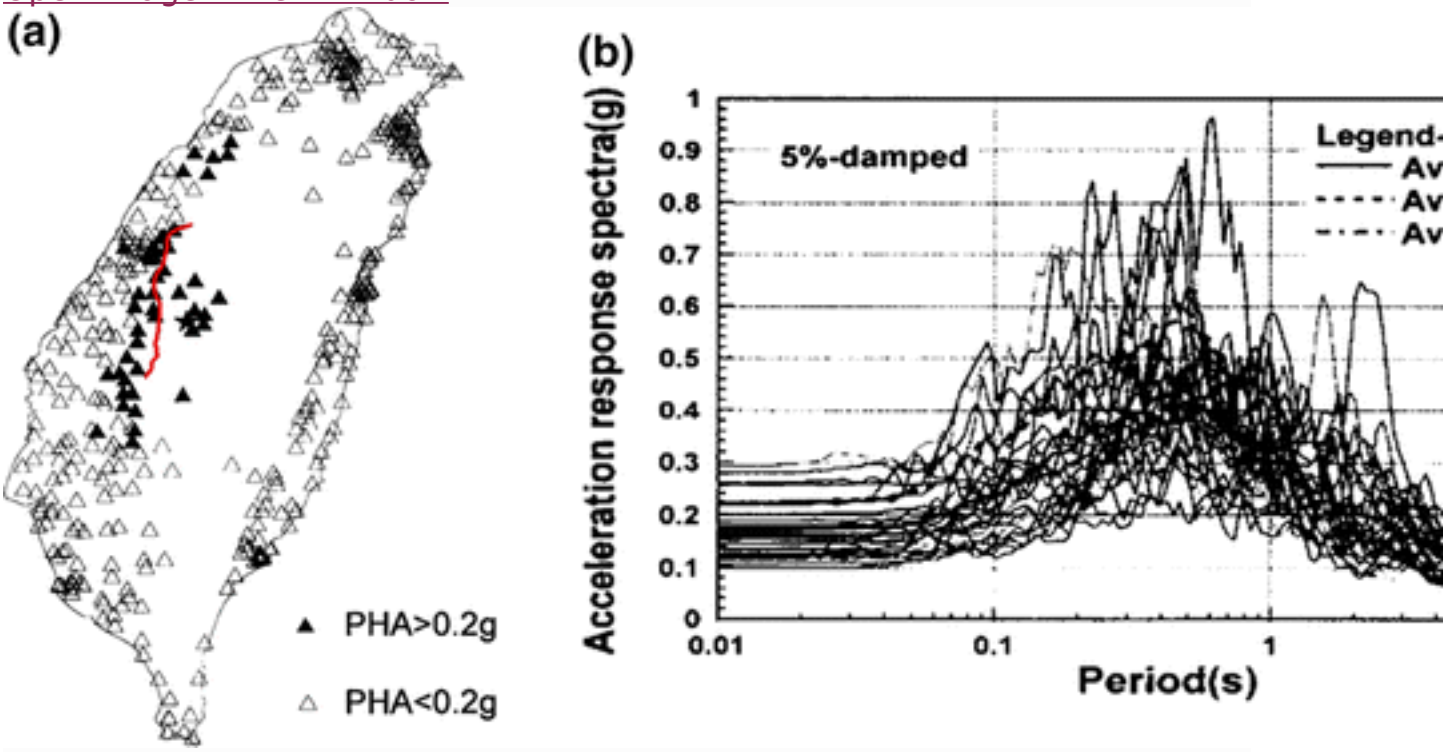

Fig. 5
a Locations (*black triangles*) near the fault (*red*) where absolute acceleration response was calculated, **b** Guo-Quan et al. (2001)
Of course, factors such as site conditions and fault type contribute to the scatter in empirical relations. Figure 6 shows peak accelerations from the M_w 7.8, Chichi earthquake plotted as function of distance. At distances of 50–100 km, variability is almost a factor of 100. This is probably primarily

due to propagation path and site response differences. This scatter is not significantly different than was observed at near-source distances for peak acceleration, suggesting that there are also many factors unaccounted for in the regression approach.

Open image in new window

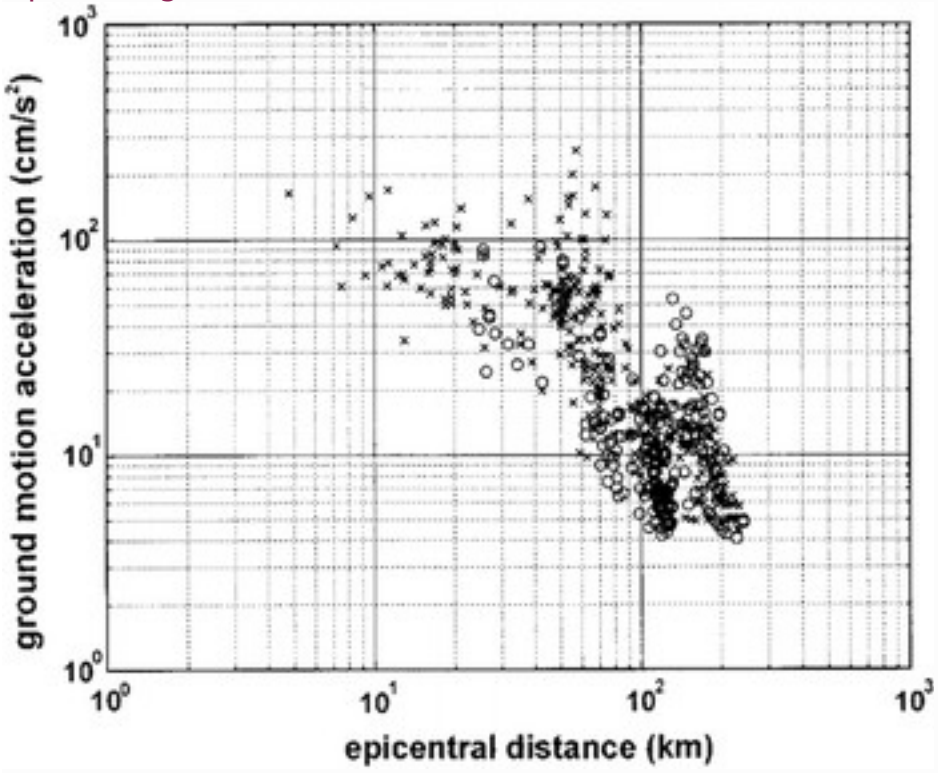

Fig. 6
Plots of peak acceleration versus distance for the $M_w = 7.9$ Chichi, Taiwan earthquake, Guo-Quan et al. (2001)

The previous examples are for individual earthquakes, referred to as intra-earthquake distributions. When different earthquakes are considered (inter-earthquake), then even greater variability can be expected. Using these results to characterize ground motion for an entirely different location (ergodic assumption) raises concerns about the validity of the hazard calculations. Strasser et al. (2009) summarize recent findings on inter- and intra-event, and inter- and intra-station variability, as well as the effect on soil nonlinearity, in peak acceleration and response spectra. Generally, there is still not sufficient data to make definitive conclusions on the relative values of these parameters. McCallen and Hutchings (1996) examined non-linear effects on buildings.

Figure 7 shows two records with the same peak acceleration used to calculate the dynamic response of a nine-story building (McCallen et al. 2015). Also shown are the lateral forces on each floor for linear and non-linear responses, which are considerably different. The Landers earthquake

caused catastrophic failure, whereas the non-linear response of the Turkey earthquake was not significantly different than the linear response.
Open image in new window

Fig. 7
Two earthquakes with similar magnitude, distance and peak acceleration, but considerably different affects on a building. From McCallen et al. (2015)

One might consider the question as to why total uncertainty (aleatory and epistemic) has not been reduced in attenuation relations over the past 50 years (Strasser et al. 2009). First, if you define epistemic uncertainty of the source as a lack of knowledge of the variables that affect the earthquake ground motion (source process, path effect and site effect) and aleatory variability as the range of unknown parameters that represent the complexity in the ground motion, then the reason is that the PSHA method depends on too simple of a formulation. An attenuation relation represented by few parameters (magnitude, distance and V_{s30} and occasionally faulting type) is not sufficient to account for the complicated processes which are controlled by many parameters. For example, representing the rise time, rupture velocity, roughness, asperities, source dimension, fault geometry and stress drop of an earthquake by one parameter (magnitude) is not sufficient to describe the process. Any variation in source parameters can significantly affect the peak values, frequency content, and spectral shape. Similarly, the path and site effects are very complicated due to the high heterogeneity in the Earth's crust and surface geology and therefore cannot be modeled by only two parameters, R and V_{s30}. Since these factors are different for each location where earthquakes occur and source process can be different for repeating earthquakes at the same location, it is not likely that there will be enough data to capture processes sufficiently to predict future hazards. Hence, each new earthquake provides new data under different conditions and the uncertainties are not reduced. To reduce the aleatory uncertainties, we must increase the number of known parameters that contribute to epistemic uncertainties, which can then be reduced with increased knowledge.

4 Performance-Based Design

One application of pb-PSHA is in performance-based design (Porter 2003). Inadequate understanding of earthquake ground motions, complexity of soil–structure interaction, and the difficulty of calculating realistic dynamic structural responses makes finding cost-effective, accurate designs difficult. Performance-based-design (PBD) attempts to meet these goals without adding extra "margins" to compensate for uncertainties, that is, PBD calculates structural responses to the predicted ground motion and designs to the calculated hazard, assuring the safety and integrity of a structure.

The need for a physics-based approach in PBD is shown from the effects at the Kashiwazaki–Kariwa Nuclear Power complex in Japan (Fig. 8) from the aforementioned M_w 6.6, 2007 Chuetsu-Oki earthquake 23 km from the facility. After analysis, the cause of the unexpectedly high ground motion was attributed partially to a focusing of ground motion by the local geology, a higher stress drop earthquake than expected, and amplifications due to site conditions (NISA 2008). A traditional PSHA would not account for any of these factors, and a pb-PSHA (with site specific Green's functions) would have accounted for all of them. Fortunately, the reactor was apparently over-designed for nuclear components and under-designed for ancillary components, so the damage to nuclear components was minimal. In a risk analysis with a pb-PSHA, the actual ground motion would have been captured in the proper treatment of the uncertain geology and tectonics of the area and this would have been used to develop a performance-based design of the facility. Then, the reactor would not be over- or under-designed for the ground motion hazard.

Open image in new window

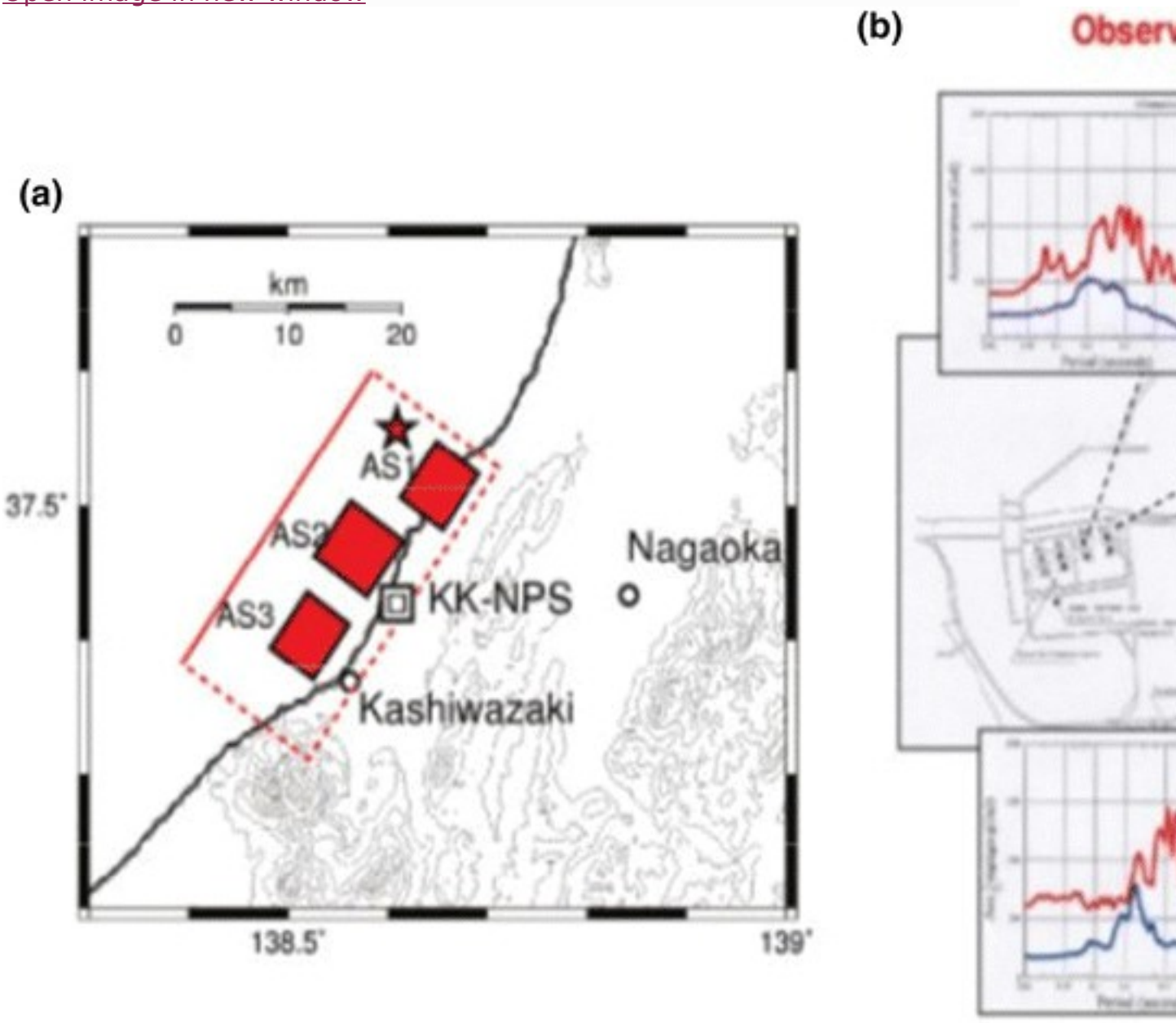

Fig. 8
a Location of the earthquake and sit of the Kashiwazaki–Kariwa Nuclear Power station (KK-NPS), calculated epicenter of the earthquake (*star*) and hypothesized location of asperities (Uetake et al. 2008), **b** absolute acceleration response curves for the design ground motion (*blue*) and observed ground motion (*red*). From NISA (2008)

5 Prediction Methodology

Our prediction methodology is based upon the work first presented by Hutchings et al. (1991, 1994) and further developed by Hutchings et al.

(1996, 2003, 2007). The physical model proposed by the previous studies has been further developed and the methodology expanded to include PSHA (Hutchings et al. 2007, Golara and Ahmady Jazany 2013; Papoulia et al. 2015; Mert et al. 2012). The full methodology is implemented by executing seven computer programs: NetMoment, HAZARD, EMPSYN, HazStats, COMPARE (discussed in Hutchings et al. 2007; Mert et al. 2014), E3D and EMERGE (discussed in Papoulia et al. 2015). Our methodology predicts a range of ground motions at a particular site that may occur from all earthquakes along specific faults or within specific source volumes and incorporates the actual geology between the source and site. We compute ground motions for finite rupture models with the Green's function summation solution of the representation relation that uses EGFs for high frequencies and synthetic Green's functions (SGFs) for low frequencies. Synthetic Green's functions may also be used for high frequency if EGFs are not available and if the SGFs are properly computed and modified for site-specific information (Heuze et al. 1997; Ioannidou et al. 2001). The same source model is used for both high and low frequencies, so merged broadband Green's functions are usable. Parameters used for modeling the source are derived from dynamic modeling and, therefore, are based upon epistemic uncertainty and provide a means for narrowing uncertainty in analysis. Below we outline this approach and demonstrate its effectiveness.

Hartzell (1978) and Wu (1978) first suggested using EGFs to calculate strong ground motions. Using small earthquakes to provide EGFs for synthesizing larger earthquakes is very practical; small earthquakes occur hundreds of times more frequently than larger earthquakes and EGFs can be readily obtained in a short period of time before a large earthquake occurs. Hartzell and Wu suggested using EGFs as the Green's function in the representation relation along with synthetic rupture processes for calculating (synthesizing) the resulting ground motion, that is, the fault of the large earthquake is discretized with elemental point sources for which EGFs are interpolated to provide the wave propagation from each point source. The rupture process is synthetic and provides the source function that is convolved with the EGFs. EGFs can also incorporate wave propagation effects that occur from different portions of a fault, so that as an earthquake ruptures, EGFs account for the different travel paths through the heterogeneous geology. Hutchings (1991) and Hartzell et al. (1999) designed particular rupture models to represent what actual an earthquake might do. This followed Boatwright (1981), who designed quasi-dynamic sources. Guatteri et al. (2003) further developed source modeling by including actual dynamic rupture processes in the calculations. In this study we discuss the point source-summation that utilizes the representation relation with a synthetic source model and either EGFs or synthetic Green's functions for wave propagation as outlined by Hutchings et al. (2007).

Of course, there are many other ground motion modeling approaches. Irikura (1986) used a relatively large earthquake as an EGF and modified it to represent the strong ground motion from an even larger earthquake (usually 1 or 2 magnitude units higher). In this approach, the EGF was not isolated as an impulsive point source, and the larger earthquake was made up of fairly large sub-events delayed and stacked to simulate finite rupture. Joyner and Boore (1986) examined the statistics of how to add up sub-events to create a larger earthquake. Frankel (1991) proposed a fractal summation of scaled EGFs to represent the source process as a statistical process. Tumarkin (1994) and Abrahamson and Bolt (1997) modified recordings of relatively large earthquakes to fit a target spectra of an even larger earthquake. Somerville et al. (1991) used the recordings near a large earthquake as an empirical source function and calculated the wave propagation effects. All these source models have different implications for the synthesis process.

The basic premises of our methodology are as follows. (1) The rupture characteristics of a fault can be constrained in advance by a range of physical parameters. (2) Accurate synthesis of ground motions for a particular fault rupture scenario, sufficient for engineering purposes, is possible from simple rupture models. (3) The range of possible fault rupture scenarios spans the limits of the earthquake process and effectively constrains the range of predictions. (4) The methodology allows one to identify the specific parameters that contribute most to the epistemic variability in the ground-motion predictions; therefore, uncertainty can be reduced with further studies.

5.1 Source Model

In our proposed methodology, rupture models are consistent with the elastodynamic equations of seismology and fracture energy and with a physical understanding of how earthquakes rupture. They also are consistent with results from laboratory experiments, numerical modeling, and field observations of earthquake processes. These models are often referred to as quasi-dynamic models (Boatwright et al. 1991). Here we refer to our model as kinematic, even though it has the characteristics of dynamic rupture.

The ultimate solution for modeling earthquakes would be a dynamic solution that satisfies elastodynamic equations and fracture energy and has known elastic constants and constituent relations for the faulting process. However, these parameters are very uncertain in the fault zone, and several poorly bounded assumptions must be used. The resulting uncertainties in computations make their usefulness limited to better understanding the earthquake process and providing bounds for quasi-dynamic rupture models.

The representation relation (Aki and Richards 2002) is the fundamental, elastodynamic, mathematical description of an earthquake and the resulting ground motion. It is expressed as

$$u_n(X,t) = \int_A m_{pq}(X',t') * G_{np,q}(X',t';X,t)\,dA \quad (1)$$

where u_n is the ground displacement in the direction $\hat{x}_n$, at location X and time t, resulting from the integral over the fault surface of the convolution of the source function $m_{pq}(X', t')$ with the derivative of the Green's function tensor $G_{np}(X', t'; X, t)$, with respect to the $\hat{x}_q$direction, at location X' and time t' on the source; * is the convolution operator and A is the fault surface. The Green's function tensor is the contribution to the displacement in the $\hat{x}_n$direction from a unidirectional unit-impulse in direction $\hat{x}_p$. A complete description of Eq. (1) can be found in the study by Aki and Richards (2002, Chapter 3), whose notation we follow. Every EGF synthesis approach utilizes this representation relation. The differences between methods are in how the equation is solved, what the source function is, and what is used for the Green's functions.

Our rupture model is implemented by the computer code EMPSYN, which calculates synthetic seismograms by numerically computing the discretized representation relation with EGF. It uses the form (Hutchings and Wu 1990; Hutchings 1991) for synthesized ground motion:

$$u_n(X,t) = \sum_{i=1}^{N} \mu_i A_i S(t')_i M_{e0i} * e_n(X,t'-t_r)_i \quad u_n(X,t) = \sum_{i=1}^{N} \mu_i A_i S(t')_i M_{0i} e * e_n(X,t'-t_r)_i \quad (2)$$

where (X,t) are position and time in space relative to the hypocenter and the origin time of the synthesized earthquake. A_i is an elemental area such that $\sum A_i$ equals the total rupture area. $\mu_i$is the rigidity at an element. $S(t')_i$ is the desired slip function at an element analytically deconvolved with the step function. This is modeled as a summation of step functions that follow the Kostrov slip function in the time domain. The time delay for the step functions' summation is at the digital sampling rate of the EGFs to ensure that high-frequency artifacts are higher than the frequency range of interest. $e_n(X,t')_i$ is the recording of a small earthquake with effectively a step source time function interpolated to have a source at the location of the ith element and origin time at the arrival time of the rupture front. t' is relative to the arrival time of the rupture front at element i; $t' = t - t_r$, where t_r is the rupture time from the hypocenter to the element, which is the integral of radial distance from the hypocenter of the synthesized earthquake divided by the rupture velocity, which can be a function of position on the fault. M_{e0i} is the scalar seismic moment of the source event and * is the convolution operator. u_n has the same units as e_n. See the study by Hutchings and Gisela (2012) for detailed discussion.

The EGF approach offers two main advantages. If the EGFs are available and managed properly, they provide the exact elastodynamic Green's function for the real earth and the exact rigidity at the source. In addition, they do not require empirical scaling relations between large and small earthquakes. If EGFs are not available, then synthetic Green's functions may also be used for high frequency if they are properly computed and modified for site-specific information (Heuze et al. 1997; Ioannidou et al. 2001).

5.2 Observations

Using empirical Green's functions, Hutchings (1994) tested source models. Figure 9 shows a simulation of an M_w 3.5 earthquake simulated with an empirical Green's function from an M_w2.3 earthquake recorded at the same stations. Both earthquakes had known moments, focal mechanism solutions, source durations and hypocenters. The Kostrov slip model, with roughness, provided the best fits to observed seismograms (Fig. 9). Further, fairly common rupture parameters were used and they produced the familiar ω^{-1} fall-off to velocity spectra (Hutchings 1994).

Open image in new window

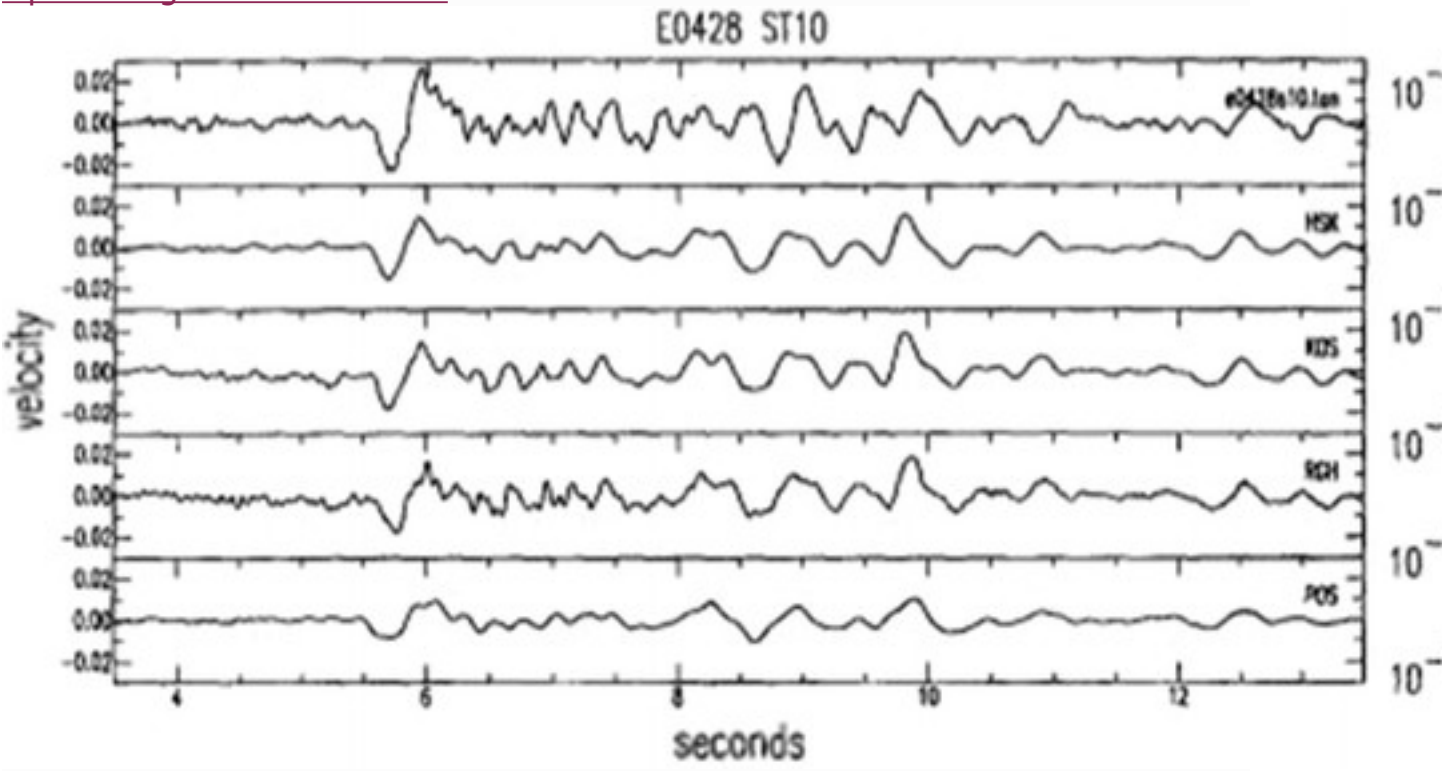

Fig. 9
Top, seismogram (*left*) and spectra (*right*) of the actual record. Followed by synthetic solutions for one component with Haskell, Kostrov smooth, Kostrov rough, rupture and point source solutions. We determined the Kostrov rough solution to be the best

This was used to model several observed seismograms. Figure 10 shows three-component seismograms modeled at two sites. The synthesized waveforms are a result of coherent phasing effects from the source constructively adding up to create the waveforms of the larger earthquake. This is not possible with random vibration Green's functions. Contributions to high frequencies in our rupture model are roughness of fault surface resulting in small asperities, large asperities, and the stopping phase of rupture (Hutchings 1991). All these contributions to high-frequency rupture are physics-based and choices can be made to span occurrences that have not yet been observed in nature.

Open image in new window

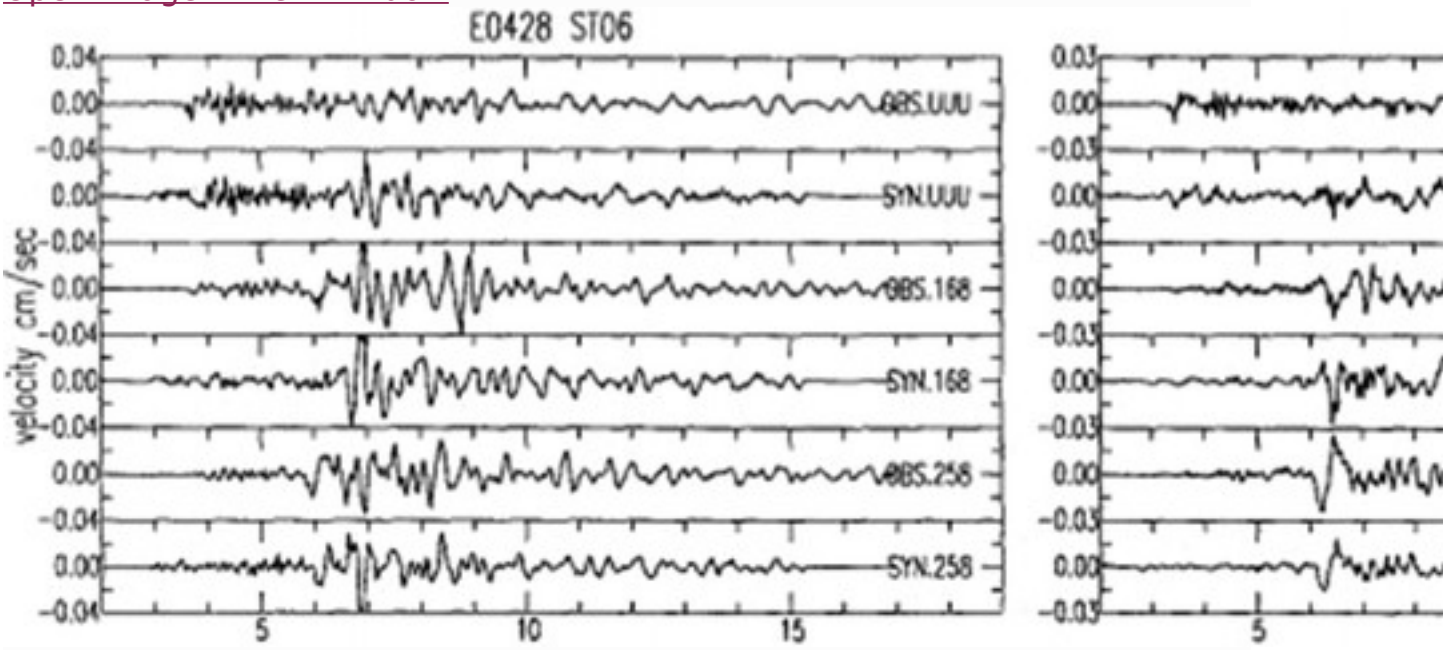

Fig. 10
Three components with actual record (*top*) followed by synthetic record at two sites

5.3 Variability in Rupture Models

The computer program HAZARD provides variability in rupture models. HAZARD randomly selects values for rupture geometry, hypocenter location, number and size of asperities, rupture and healing velocity, and rupture roughness from even distributions. Strike, dip, and slip vector selected from triangular distributions are about preferred values. Moment of an event is chosen from *b* values for each fault or source zone. Rise times, stress drop, and energy are dependent variables. We use data from summary studies to constrain some parameters (identified below). Although it is our desire not to depend upon regression of past earthquakes for modeling, some parameters may well be characterized using the ergodic assumption (Wells and Coppersmith 1994; Somerville et al. 1999).

Geometry is rectangular for faults that rupture through the entire crust; otherwise, it is elliptical. The shape is determined by examining the slip distributions of previous earthquakes (Hartzel, many references; Wald, many references). Elliptical geometries vary in eccentricity between 0.0 and 0.95. Any shape of rupture surface can be used if desired.

Slip distribution is varied in two ways. First, the Kostrov slip model with healing (Hutchings 1994) has variable rise times and slip amplitudes on the fault but constant stress drops. As a result, portions of the fault have high slip amplitudes. Second, smaller areas with high slip amplitudes and high stress drops are modeled. These areas, called asperities, are not permitted to overlap. Fault displacement for asperities grades from the value of background rupture at the edge to greatest at the center. The range for our models is between 10 and 40% of the total fault area. Somerville et al. (1999) examined slip distributions from inversion results, primarily from Hartzell and/or Wald (many references), to characterize slip distributions and found that slip amplitudes greater than 1.5 include 20.67% of the total fault surface from regression with all of their data. We can use this as a guide or allow rupture models to vary in any degree we wish.

Asperities are circular in shape and have slip distributions defined by the Kostrov rupture with healing. The number of asperities is randomly chosen to be between 0 and 7. Although the number of asperities is roughly independent of the size of the earthquake, their relative size scales with fault dimension. This process replicates observation with inversion studies, which indicates that relatively small asperities are not significant to the ground motion of larger earthquakes. The slip amplitude of the asperities is controlled by the Kostrov slip function from their stress drop. Of course, any number of asperities can be used as desired.

Rise time varies at each point on the fault and is a dependent variable. Rupture initiates at the arrival time of the rupture front. It continues for the shortest amount of time it takes the rupture front to reach a fault edge and a healing phase to travel back to that point at the healing velocity. Healing phases are not permitted from the surface where there is little seismogenic rupture. Our healing model is derived from dynamic rupture models (Tse and Rice 1986; Das and Kostrov 1990; Guatteri et al. 2003; Tullis et al. 2012) and several others.

Rupture roughness is the percentage of elements at the rupture surface for which we apply randomness to the rise time to simulate roughness. The percentage is randomly selected to be 0, 10, 20, 33, or 50%. For this percentage of elements, rise time is randomly shortened to be between 0.1 and 0.9 times the original value. Roughness is implemented by delaying an element’s rupture time so that it finishes slip (rise time) at the same time as

neighboring elements. Areas of roughness have corresponding high stress drop [i.e., Schulz's (2002) model of contact asperities]. Asperities and background features have the same percentage of elements with roughness.

Rupture velocity is permitted to vary between 0.75 and 1.0 times the shear-wave velocity as derived from dynamic rupture modeling (Das and Kostrov 1990 and several others). "Super shear" rupture up to the P-wave velocity can be used if desired.

Healing velocity is a percentage of the rupture velocity. If the healing velocity is greater than the rupture velocity, it will shortly overtake the rupture front, and no rise time will develop. We randomly vary healing velocity to be between 0.8 and 1.0 times the rupture velocity, which is approximately between the Raleigh-wave velocity and the shear-wave velocity as observed in dynamic rupture modeling.

Stress drop is a dependent variable derived from the Kostrov slip function. In this derivation, stress drop is that which results in a strain discontinuity and a displacement on the fault, resulting in seismic radiation. It is equivalent to the Orowan stress drop (Orowan 1960). Our kinematic models use four effects to vary stress drop in rupture. First, the overall average stress drop is directly dependent on the moment and size of the rupture area. Second, rupture roughness (described above) results in small areas of relatively high stress drop. Third, asperities are allowed to have a different stress drop than surrounding portions of the fault rupture, and fourth, stress drop is constrained to diminish near the Earth's surface at the rate of 10 + 0.75 times the confining pressure due to lithostatic load (300 bars at 1.7 km depth). The minimum of either this value or the full rupture stress drop is used. Typically, stress drop for the main event ranges from 1 to 100 bars, while asperities range from 50 to 500 bars.

Rigidity and stress drop are reduced proportionally near the surface in relation to lithostatic load. Reducing the rigidity results in very little moment contribution for rupture near the surface. Additionally, the commensurate diminishing of stress drop and rigidity results in significant displacements (although not significantly seismogenic) at the surface.

Hypocenter depth is limited to be within the lower half of the rupture area because large earthquakes are theoretically predicted to nucleate at depth (Tse and Rice 1986). Hypocenters also must be greater than the distance from a fault edge to limit strain to be less than 10^{-1}, generally greater than 100 m.

Energy is calculated for each fault rupture model by the integral of slip amplitude and stress drop (Tumarkin 1994) to identify possibly unrealistic

models as suggested by Tullis et al. (2012). We used calculations of the effective stress as the ratio of moment to energy to identify rupture models that have unrealistic energy values. Models are allowed to have effective stress values between 0.05 and 50 MPa. This range is considered broad enough that it does not eliminate any possible extreme events but will limit unrealistic events. Generally, we do not find unrealistic events with our rupture models.

5.4 Physical Limits to Dynamic Rupture

A significant question in simulations of dynamic rupture and choosing parameters is whether one can limit the parameter range. Certainly, some parameters have obvious limits—for example, the number of large asperities is limited by the moment budget. The total moment also limits the amplitudes of synthesized seismograms. Following Joyner and Boore (1986) and Hutchings (1994), it was shown that a simple form of the Fourier amplitude spectrum could be developed if it is assumed that Green's function's Fourier amplitude spectra are similar at a particular recording site, even if their phase spectra are quite different. If this is the case, the Fourier amplitude spectrum of the synthesized seismogram can be expressed as:

$$|U(\omega)|=|E(\omega)|\frac{\sum_{j=1}\eta\kappa 2j+\sum_{j=1}\eta\sum_{k=1j\neq k}\eta\kappa j\kappa k\cos(\varphi j-\varphi k+\omega\tau k-\omega\tau j)}{\sum j=1\eta\kappa j2+\sum j=1\eta\sum k=1j\neq k\eta\kappa j\kappa k\cos(\varphi j-\varphi k+\omega\tau k-\omega\tau j)},|U(\omega)|=|E(\omega)| \quad (3)$$

where $\kappa=M_{j0}M_{e0}\kappa=M0jM0e$ is the moment of each element divided by the moment of the EGF for that element, ωω is angular frequency, $\phi(\omega)\phi(\omega)$ is the phase spectrum of the Green's function, and τ is element rupture. Scaling effects and the effects of different rupture parameters on the Fourier amplitude spectra are fairly easy to observe. At low frequencies, → 0, the phase spectrum and rupture time of Green's functions is the same, and the spectral amplitudes are expressed as:

$$|U(\omega)|=|E(\omega)|M0M_{e0}.|U(\omega)|=|E(\omega)|M0M0e. \quad (4)$$

Equation (4) is an expression for the largest spectral amplitudes possible for the synthesized seismograms at low frequencies. The phase effects of different Green's functions modulate spectra at higher frequencies. This means that the frequency content of synthesized seismograms (and actual recordings as well) is dependent on the constructive and destructive interference effects caused by the rupture parameters and spatial variation of the Green's functions. Hutchings (1994) showed that this results in a general ω^{-1} fall-off to velocity spectra when traditional values are used. However, it is not confined to that and can differ for very near-source locations or extreme or unusual combinations of rupture parameters. In fact

(and for ours too), it is easy to match the ω-squared model in the far field in as long as the source model has a fractal distribution ($D = 2$) of high frequency (Frankel 1991). If rupture parameters reach their highest values, i.e., rupture velocity approaches values such that the duration is effectively instantaneous and rise times approach values such that they are effectively zero for the frequencies of interest, then the phase effect goes to zero and the highest amplitudes that are reached are also expressed by Eq. 4. For frequencies of interest, say 25 Hz, the limit for stress drop is high, but bounded. Therefore, even high values of rupture velocity, or other time-dependent rupture parameters have physical limits that, in turn, limit the amplitudes of synthesized seismograms.

5.5 Pore Pressure and Dynamic Rupture

Miah (2016) ran dynamic rupture of earthquakes with PyLith (Aagaard et al. 2013) and examined the effect of fluids. He found the added pore pressure due to fluids results in a reduction of the tectonic stress necessary to initiate an earthquake and affects the recurrence rate of seismicity [PSHA element (2) above], thus hazard estimates must account for variations in recurrence rates due to fluids.

Miah (2016) ran three simulations of an $M_w \sim 4$ earthquake to demonstrate the effect of pore water pressure on the dynamic rupture of a fault defined by rate- and state-dependent friction law. The results from the dynamic response analyses showed that in the presence of fluid-induced pressure, dynamic rupture nucleated by a factor of almost 10 times earlier. Even with a reduction of pore water pressure of a factor of approximately 4, fluid-influenced dynamic rupture nucleated by a factor of almost 2 times earlier.

6 Green's Functions

6.1 Empirical Green's Functions

Propagation complexities are not well captured by crustal models, which provide the basis for calculating synthetic Green's functions. At high frequencies (>1 Hz), wave propagation is very sensitive to small crustal heterogeneities, which are generally not well known; at low frequencies (<1 Hz), wave propagation can be modeled fairly accurately. EGFs can be used instead of mathematical calculations to more accurately represent seismic wave propagation in the geologically heterogeneous crust. The EGF method is the best available method because it empirically corrects for unknown path and site effects, for which a short wavelength resolution is needed. However, true EGFs contain the source rupture process of the small earthquakes in the recorded seismograms. No earthquake has a true impulsive source. Therefore, one must be careful using EGFs. Hutchings et

al. (2007) demonstrated how to utilize slightly larger earthquakes ($M_w \sim 3$) as point sources in the solution. Other factors also need to be considered. Wossner et al. (2002) researched the effects of a limited number of Green's functions and variations in moment calculations, Hutchings and Wu (1990) researched the effects of variations in focal mechanism solutions and interpolation, and Hutchings et al. (2007) incorporated their effects into uncertainty of the solution. Pavic et al. (2000) examined uncertainties when using empirical Green's functions.

EGFs are theoretically from impulsive point sources, which in our application require the rupture duration of the source event to be short enough that the source corner frequency is higher than the highest frequency of interest. Generally, such small earthquakes are not available. Hutchings et al. (2007) utilized earthquakes $M_w \sim 4$ as EGFs by deconvolving out a Brune source model to provide effective impulsive point sources. Figure 11 shows acceleration records and their displacement spectra prior to such a correction and after the correction has been implemented. Golara and Ahmady Jazany (2013) confirmed this approach. They deconvolved out a Brune source model from records from events with magnitude $4.0 < M_w \leq 5.0$ to minimize finite source effects. Golara and Ahmady Jazany (2013) point out that the Brune source has zero phase shifts so that in the deconvolution only the amplitude spectra are affected. In Fig. 11, after a point source correction, the site response remains. It is apparent that the site response is significantly different at each site location. Unfortunately, EGFs do not include the effects of material nonlinearity caused either by modular damping and reduction or by loss of effective stress (liquefaction). This has been addressed by Heuze et al. (1997).

Open image in new window

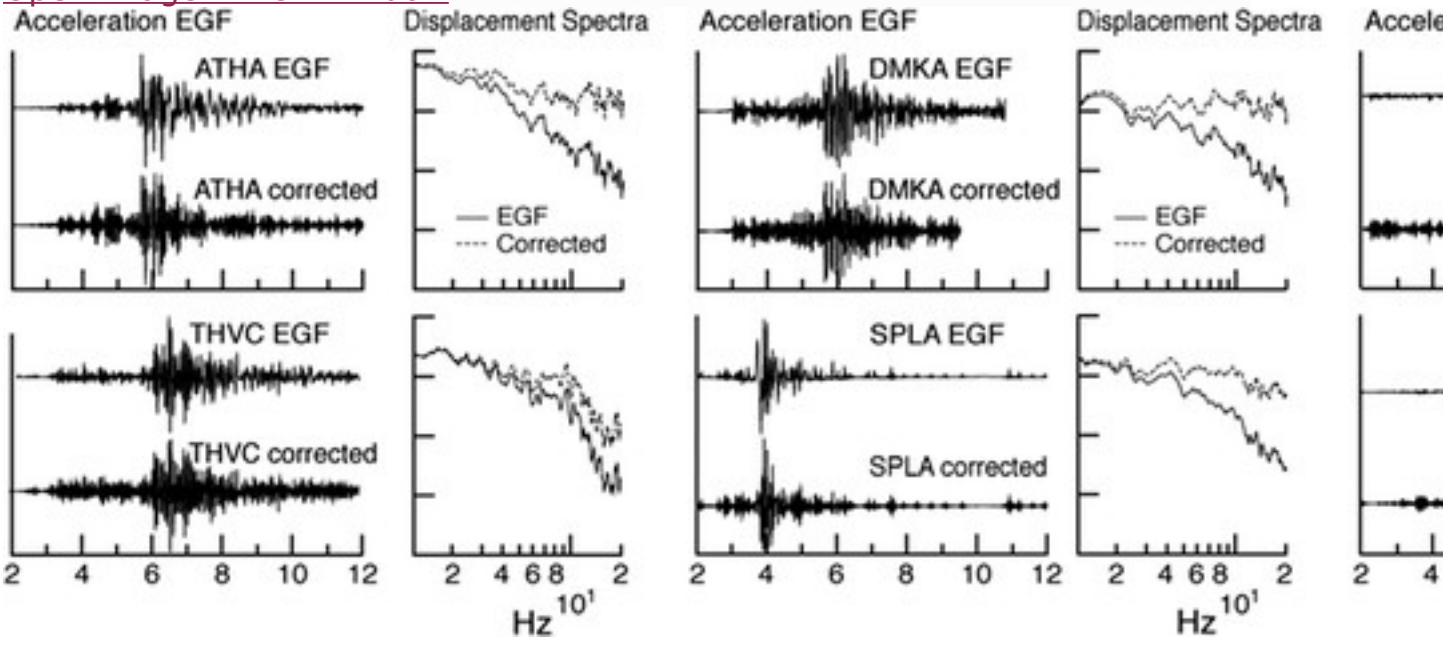

Fig. 11
Correction to accelerograms to create effective EGFs at six sites that recorded the 1999 Athens earthquake

There are several limitations to EGFs. The selection of an EGF for use in source studies follows strict criteria that are not always possible to fulfill. Thus, a suitable EGF function may not be available, limiting the number of earthquakes that can be analyzed. The bandwidth of the EGF for which enough signal above noise is available is another limiting factor in source studies. For very small EGF earthquakes or noisy surface stations, the available bandwidth may not be enough to perform the source analysis, even though there is sufficient signal from the earthquake being analyzed. Limited instrument bandwidth, another potentially serious limitation, may bias the source parameters. However, the EGF method profits from having a good distribution of recording stations, providing a good azimuthal coverage so that source directivity effects may be accounted for.

There are also a number of limitations in applying EGF methods to ground-motion modeling: (1) in virtually all practical applications, there is insufficient number of EGFs to provide an impulse response for all portions of a fault rupture to be modeled. (2) EGFs cannot accurately model variations in focal mechanism solutions. (3) Noise levels in recordings limit their usable frequency band (usually between 0.2 and 25.0 Hz or narrower) necessary to ascertain the locations and source parameters of the small earthquakes that would provide EGFs. (5) Good-quality recordings of seismograms have to be captured at the locations of interest for ground-motion synthesis.

6.2 Synthetic Green's Functions

Green's functions at low frequencies (<1 Hz) can be accurately calculated because the geology is often known well enough to be accurately modeled with a coarse spatial resolution. Papoulia et al. (2015) demonstrated the application of synthetic Green's functions. Novikova (personal communication, 2015; *National Observatory of Athens*) utilized the explicit 2D/3D elastic finite-difference wave propagation code (Larsen and Schultz 1995) to synthesize Green's functions for frequencies less that 1.0 Hz in a study of the Saronikos Gulf, Greece.

Synthetic Green's functions may also be used for high frequency if EGFs are not available and if they are properly computed and modified for site-specific information (Heuze et al. 1997; Ioannidou 2001).

6.3 Merging High- and Low-Frequency Green's Functions or Synthesized Seismograms

Fahjan (personal communication, 2013; *Gebze Technical University, Istanbul, Turkey*) developed an algorithm to merge low- and high-frequency simulated motion broadband solutions. The sampling rate of the earthquake records used as EGFs in the high-frequency band is 0.02 s, thus providing high-frequency components up to 25 Hz Nyquist frequency in the spectra. However, because of the noise level characteristic of the smaller size earthquakes, the preferred frequency band was selected as 0.5–20 Hz and in the merging algorithm 0.5 Hz was used as the pivot frequency. The GF synthetics at low frequencies (0.1–0.5 Hz) calculated using finite difference algorithms yield reliable results by taking into account the grid size (0.5 km) and the structural features of the seismic velocity model. The two components are combined at a merging corner frequency with a low-cut filter applied for low-frequency motion records and a high-cut filter for high-frequency motion records. The code used an optimization process to select proper filtering coefficients such that the sum of the merged filtering function in the frequency domain would be approximately unity (Fig. 12). Figure 13 shows merged records.

Open image in new window

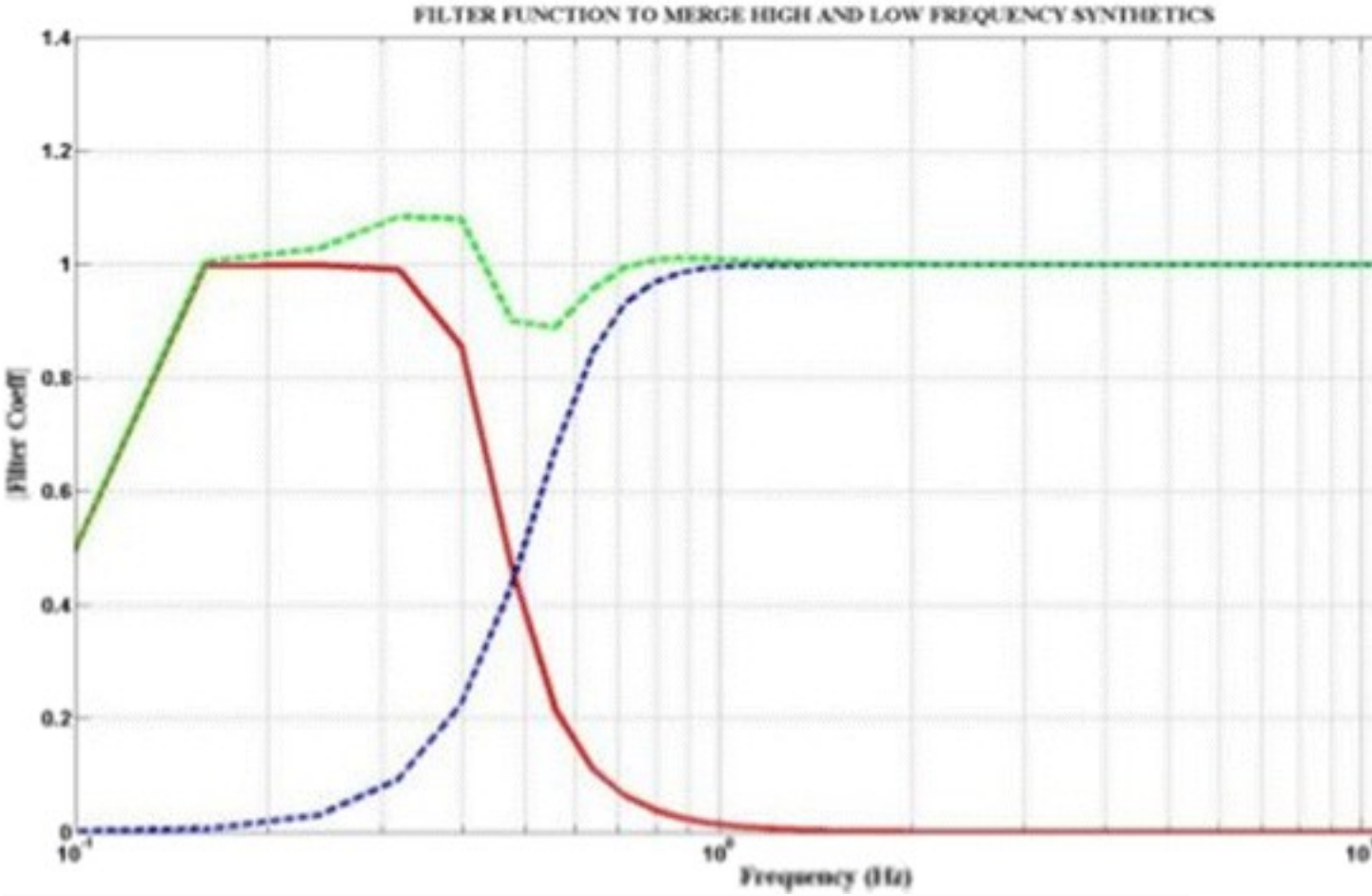

Fig. 12
The filter functions used to obtain the broadband earthquake simulations

Open image in new window

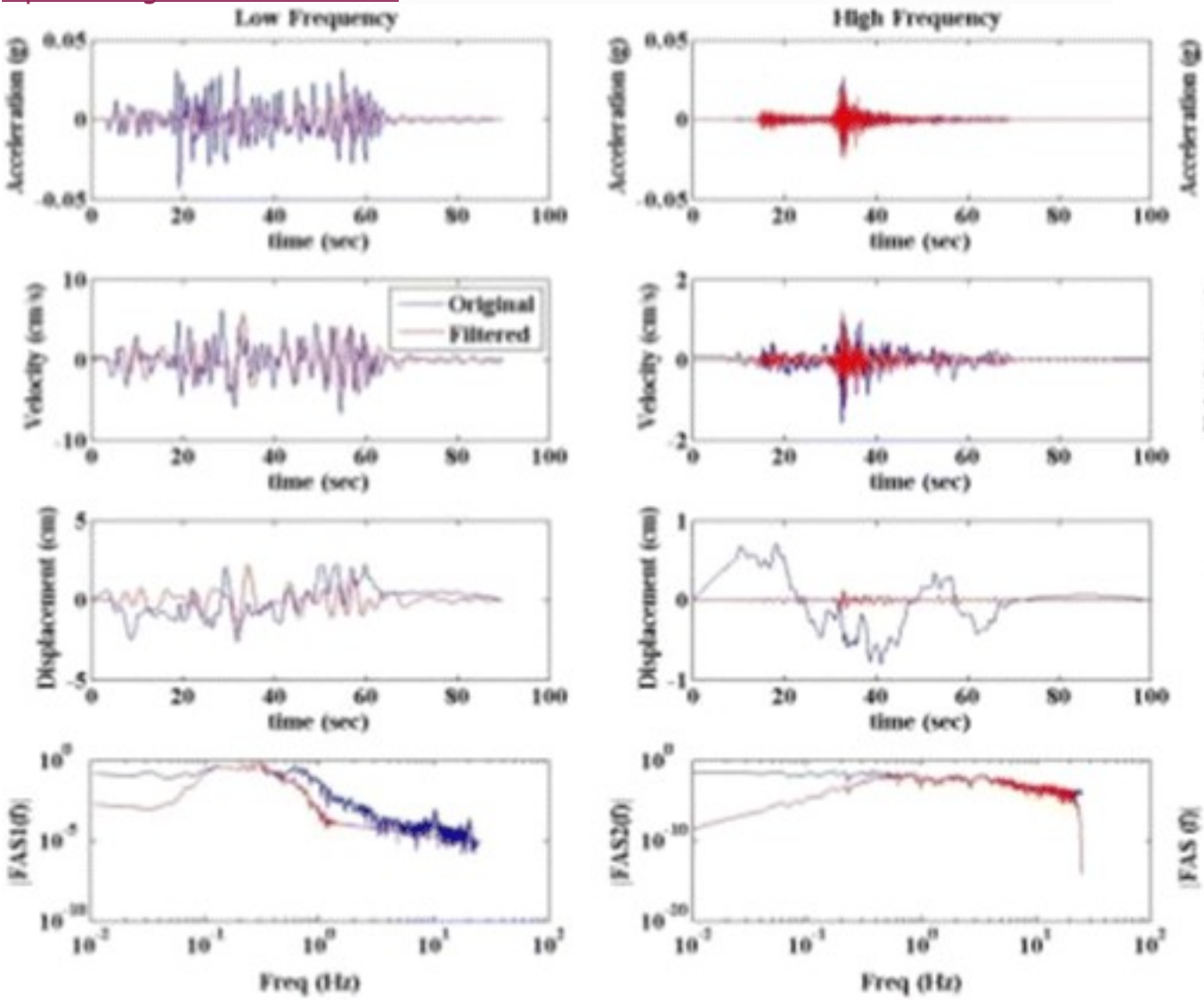

Fig. 13
Integration of the simulation results obtained for low- and high-frequency bands at YLV station (*blue color* is the original seismogram, while the *red color* is the filtered seismogram)

As a consequence, the frequency content for the merged output records in the vicinity of the merging corner frequency did not have spurious amplitudes. The fast Fourier transform (FFT) scaling procedure with a given harmonic motion for different frequencies and amplitudes was checked and gave the exact amplitudes at the given frequencies. The blue seismograms in the first column of Fig. 13 are the low-frequency SGF simulations while the red seismograms are the filtered simulations derived using the filter function shown in Fig. 12. The second column shows the high-frequency original and filtered simulations and the third column indicates the original and the

filtered seismograms obtained from the low- and high-frequency components of the simulations.

7 Validation

The methodology has been validated several times by comparing to past earthquakes (Hutchings et al. 1991, 1994, 1997, 1998, 2007; Papoulia et al. 2015; Hutchings and Wu 1990; Foxall et al. 1996; Hutchings and Jarpe 1996; Jarpe and Kasameyer 1996; Wossner et al. 2002; Scognamiglio and Hutchings 2009; Mert et al. 2011). Scognamiglio and Hutchings (2009) showed that by constraining source parameters from independent studies for the 1997 Colfiorito earthquake, uncertainty bounds were reduced by a factor of almost two and the actual earthquake parameters were still described by the uncertainty bounds. Foxall et al. (1996) fixed the moment, focal mechanism solution, slip distribution, and geometry from independent studies and modeled the observed strong ground motion at 26 sites. Jarpe and Kasameyer (1996) found that the standard error between observed and predicted response spectra is less than or equal to other methods for periods between 0.05 and 2.0 s and is significantly less than regression methods based on pre-Loma Prieta empirical strong motion data at periods between 0.5 and 5.0 s. Mert et al. (2011) made an assessment of uncertainties and confidence level in the selection of rupture parameters.

The computer code for EMPSYN has been validated by synthesizing an idealized earthquake with the same parameters used by a similar synthesis approach conducted at the University of California, Santa Barbara (UCSB) (Liu 1999, personal communication; *University of California, Santa Barbara*). Liu's results were essentially identical to the EMPSYN calculation. Hutchings (1994) also synthesized an expanding circular crack solution which matched the analytical solution.

Golara and Hamzehloo (2006) tested the potential of the approach discussed here as a prediction tool. The analysis was carried out for the 2004 Firoozabad–Kojoor earthquake. Thirty possible rupture models for the Kojoor fault were generated to account for source variability. These models were based on a previous study of this area without including knowledge of the source characteristics following the occurrence of the earthquake. Golara and Hamzehloo (2006) found that the actual ground motion recordings fell within the range of synthesized ground motions. Figure 14 shows the observed and synthesized ground motion for the best-fitting model. If all models for the causative fault had been utilized to calculate the risk to structures, then the amplitudes, frequency content and phasing of the actual ground motion would have been well represented in the suite of calculations.

Open image in new window

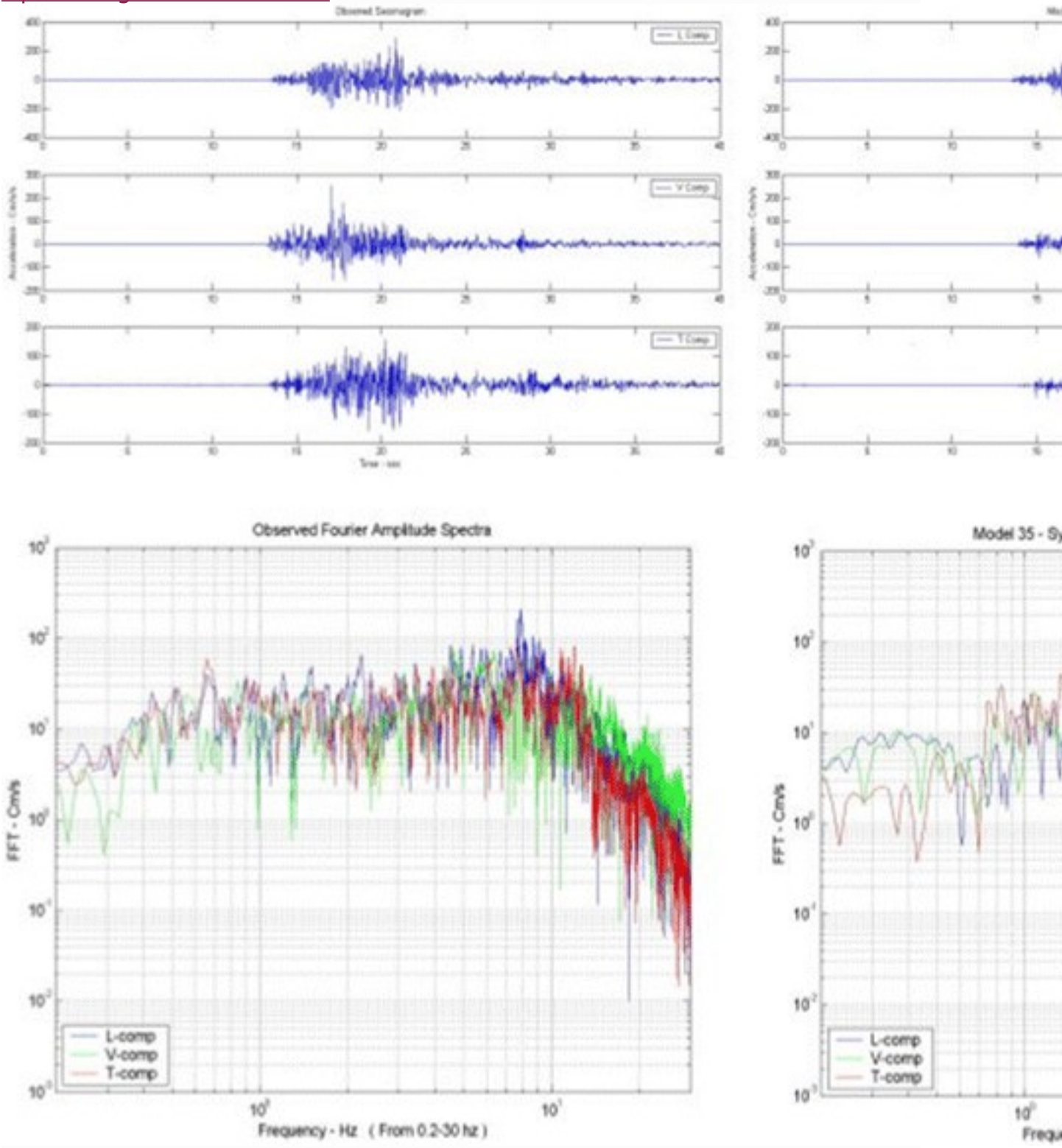

Fig. 14

Observed three components of ground motion and the Fourier spectra (*left*). Synthesized ground motion and Fourier amplitude spectra (*right*) for the best model

Golara and Ahmady Jazany (2013) modeled strong ground motion and design spectra for an M_w 7.0 earthquake that may occur in the future along the north Tehran fault, 20 km from the center of the metropolitan area of Tehran. Previously an M_w 4.1 earthquake occurred on the fault, the closest earthquake to Tehran ever recorded. Golara and Ahmady Jazany (2013) created twenty source models by varying source parameters. They found that the 5% dampened response spectra had good agreement with the range of spectral accelerations predicted by the attenuation law developed by Campbell and Bozorgnia (2003). Golara and Ahmady Jazany (2013) concluded that this approach provides a means to predict ground motion without the need for attenuation relations. Mert et al. (2010, 2011) simulated five mid-sized earthquakes that occurred in Marmara Sea region: four M_w 5.0 and one M_w 4.9. Figure 15 shows the location of the five earthquakes and the smaller earthquakes used to provide EGFs, including the stations where the records were synthesized. Mert et al. applied the test proposed by Anderson (2004) to determine whether synthesized seismograms fit observed records for engineering purposes. The test included ten engineering attributes and displacement, velocity, and accelerative records. A cumulative score of 0–100 was used to evaluate the results. Figure 16 shows results for the M_w 5.0 Kus Lake earthquake for four of the attributes at five stations. The “Anderson Score” for all attributes is 85. Reading across for each station are results for spectral displacement, pseudo-velocity response, pseudo-acceleration response, and absolute acceleration response. The five earthquakes had Anderson Scores of 68, 73, 82, and 64 (Fugro-Earth 2001). Anderson (2004) considers scores above 60 to be good and above 80 to be excellent.

Open image in new window

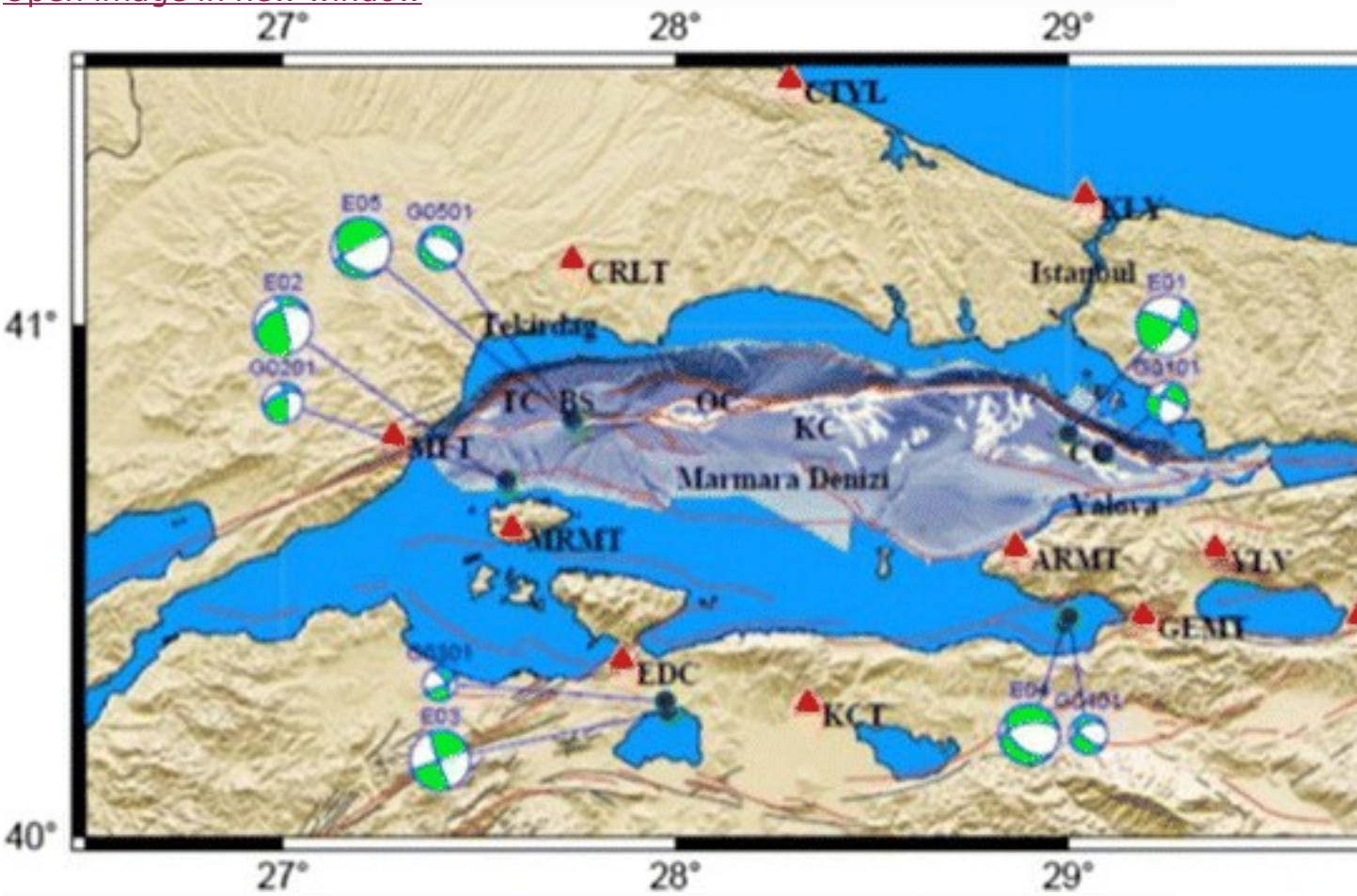

Fig. 15
Events synthesized (*larger focal spheres*) and the events used to obtain EGFs (*smaller sphere*). Stations where the records were synthesized are plotted as *red triangles*

Open image in new window

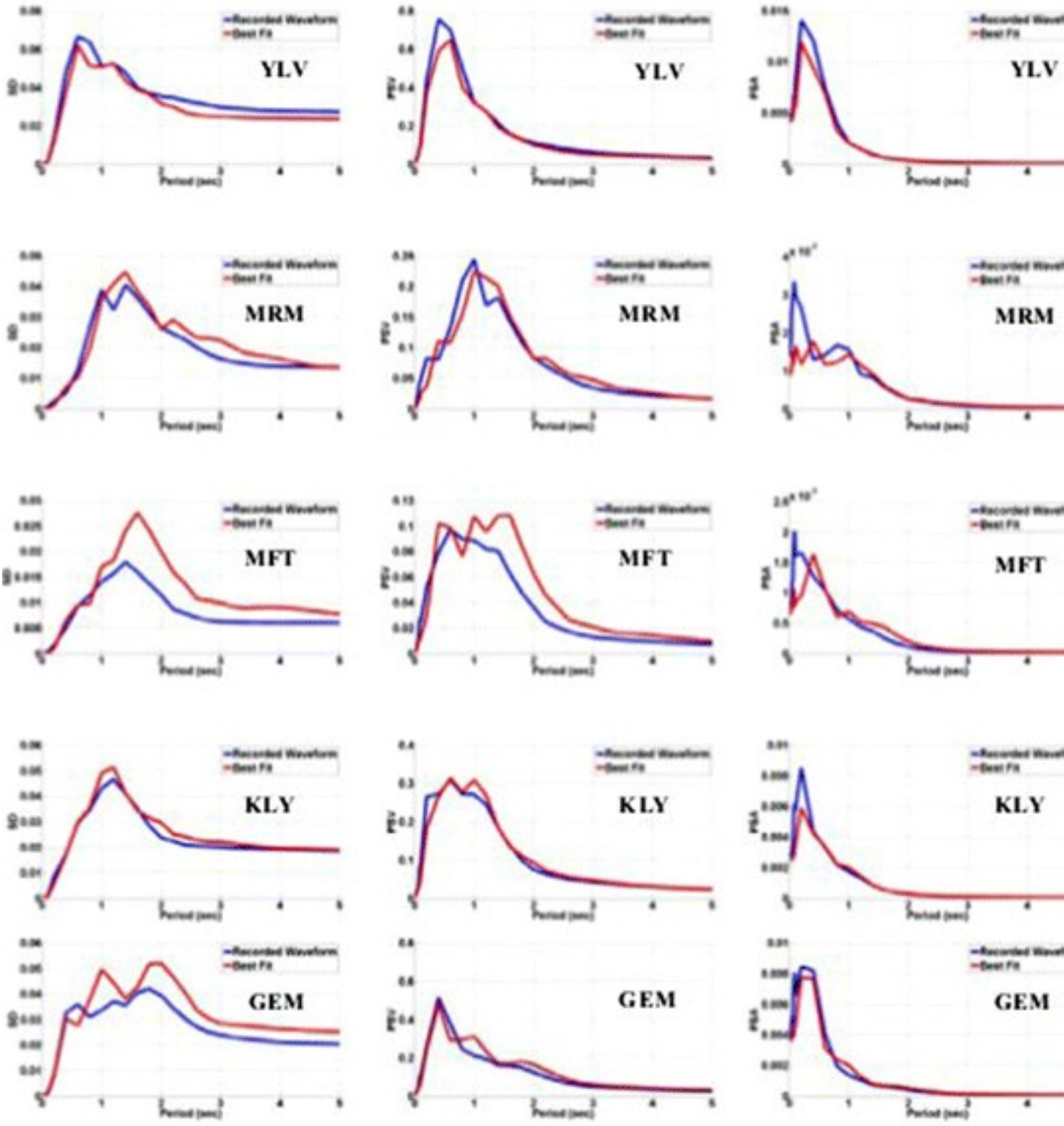

Fig. 16
Results for the M_w 5.0 Kus Lake earthquake for four of the attributes at five stations

Fergany and Hutchiings (2017) demonstrated the pb-PSHA methodology with the ground motion simulation of M_w 5.5, 1998 Ras-Elhekma earthquake in northern Egypt. The boundaries for the possible rupture parameters that may have been identified prior to the 1998 Ras-Elhekma earthquake were estimated. Rupture parameters are randomly varied by the program HAZARD (Hutchings et al. 2007) to create 500 scenarios. Fifty models from the larger set of 500 scenarios were used to test the prediction hypothesis within the possible source volume for the 1998 event. The best rupture models were identified based on the goodness of fit between recorded and simulated seismograms at three sites that recorded the earthquake using Anderson's (2004) method. The best model occurred in the vicinity of 31.40°N, 27.69°W, with a nearly bilateral center of rupture at 22.78 km depth. Strike was N326.7°E, dips ranged around 43.7°, rupture velocity 0.85Vs, and healing velocity 0.86Vr. The best rupture scenario of the 1998 earthquake was then used to synthesize the ground motions at sites where the main shock was not recorded. The site-specific character was taken into consideration by the Empirical Green's Function and the geometric relationship to the source rupture. The EGFs were provided by deconvolving out the finite source effects of the aftershocks (M_w 4.0) that were larger than the criteria for having impulsive point sources to generate impulsive point source EGFs.

8 Application

One of the important steps in the development of the methodology was to extend it to all significant magnitudes for a PSHA in the northern area of the Saronikos Gulf, Greece (Papoulia et al. 2015). Papoulia et al. examined the E–W striking Aigina fault, which is capable of producing earthquakes of M_w 6–6.5 (Papanikolaou et al. 1988; Kiratzi et al. 1985; Makris et al. 2004a, b). An earthquake of this magnitude could be catastrophic for the Saronikos Gulf region, which is the most densely populated coastal part of Greece and has the highest concentration of industrial activity and critical infrastructure.

The important aspect of the study was to combine the basic PSHA with broadband ground motion simulations to obtain broadband hazard analysis for all significant magnitude earthquakes, and provide the necessary simulated ground motions to calculate building response and, therefore, risk.

Papoulia et al. (2015) used a range of rupture scenarios for all significant magnitude earthquakes along the Aigina fault. The hazard calculation was for frequencies 0.0–15.0 Hz. Recordings of small earthquakes from an onshore/offshore local seismic array were used as EGFs for frequencies of 1.5–15.0 Hz. The finite difference code E3D (Larsen and Schultz, 1995) was utilized to synthesize SGFs for frequencies 0.0–1.5 Hz and an algorithm for merging the EGFs with SGFs was also employed.

Papoulia et al. (2015) calculated seismograms for 600 rupture scenarios and for earthquakes with M_w 3.5–6.5. The library of the seismograms was the basis of the hazard study and could be important for non-linear dynamic analysis of structures in the coastal zone and the potential hazard to long-period structures.

Papoulia et al. (2015) assumed they synthesized a sufficient number of earthquakes that represented the full range of possible rupture scenarios from this method, but not every earthquake. This assumption required a sufficient time period for several cycles of the earthquake to occur at any particular location along the fault. Papoulia et al. (2015) assumed an average return period of 1000 years for the largest magnitude earthquakes in this particular source zone and included many cycles of smaller earthquakes. From this, a catalog of ground motion for a period of 100,000 years was simulated. They obtained a distribution of traditional ground-motion parameters (such as peak acceleration) or spectral ordinates from the synthesized ground motions and developed hazard curves in the form of the annual probability of exceedance. The example of the results of PSHA is given in Fig. 17.

Open image in new window

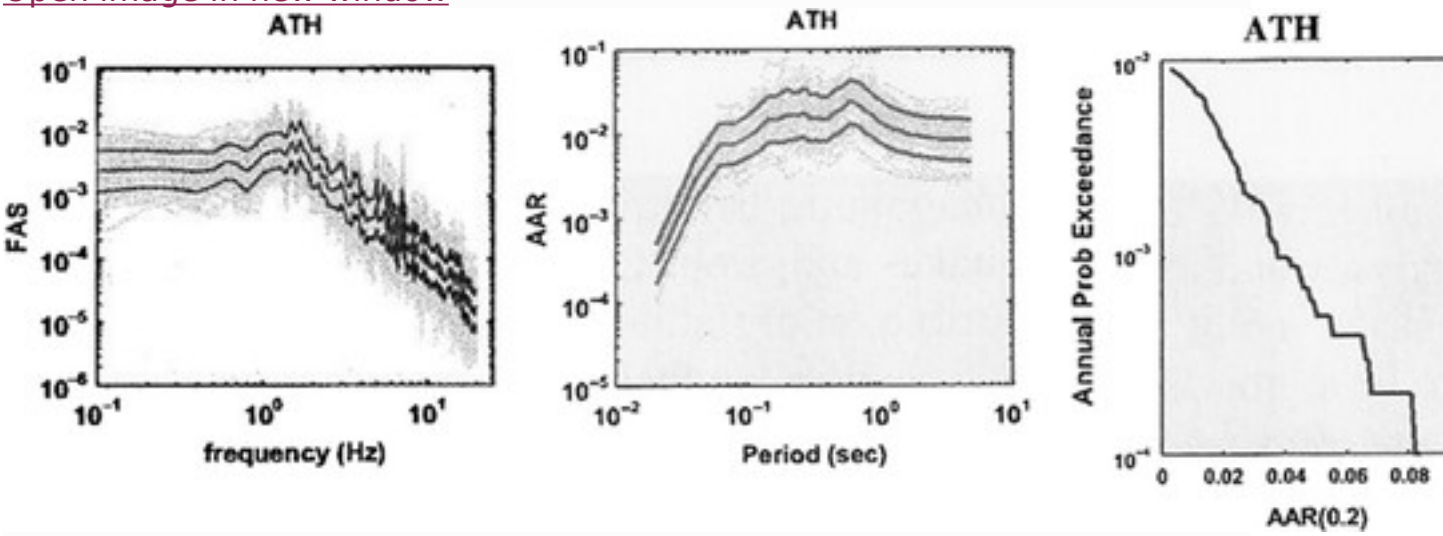

Fig. 17
Fourier amplitude spectra (N–S component); absolute acceleration response (N–S component) calculated for 600 scenarios; annual probability of exceedance from the 0.2 s; uniform hazard curves. ATH is the station located NE from the fault

Another application illustrates the advantage offered by physical-based models, especially when calculations are applied directly to structures without the filtering effect of regression relations. Hutchings et al. (1996) modeled ground motion that may have occurred in the un-instrumented area of the interchange between California State Highway 15 and Interstate

I-5, which failed as a result of the 1994 Northridge, California, earthquake. Synthesized ground motions utilized empirical Green's functions recorded at the interchange. The synthesized seismograms were used to analyze the failure of the structure and possible replacement designs (Fenves and Ellery 1998). The synthesized seismograms included a large fault-normal pulse that resulted in an extra "bump" at about 1 s in the pseudo-acceleration response spectra. This bump was not considered by other empirical-based methodologies and was not observed by nearby acceleration sites that were not on the strike of the fault (Figs. 2.18 and 2.19 in Fenves and Ellery 1998).

Another application was to "predict" the ground motion that may occur at the San Francisco–Oakland (California) Bay Bridge (SFOBB) from an M_w 7.25 earthquake along the Hayward fault (Hutchings et al. 1996, 2005). Several source models resulted in long-period, fault parallel tectonic "fling" pulse shapes that had not been previously considered because they had only occurred once prior and had previously been filtered from strong motion records. McCallen et al. (2006) found that these pulse shapes would have caused damage to the eastern span of the San Francisco Bay Bridge using a finite element model of the bridge (Fig. 18).

Open image in new window

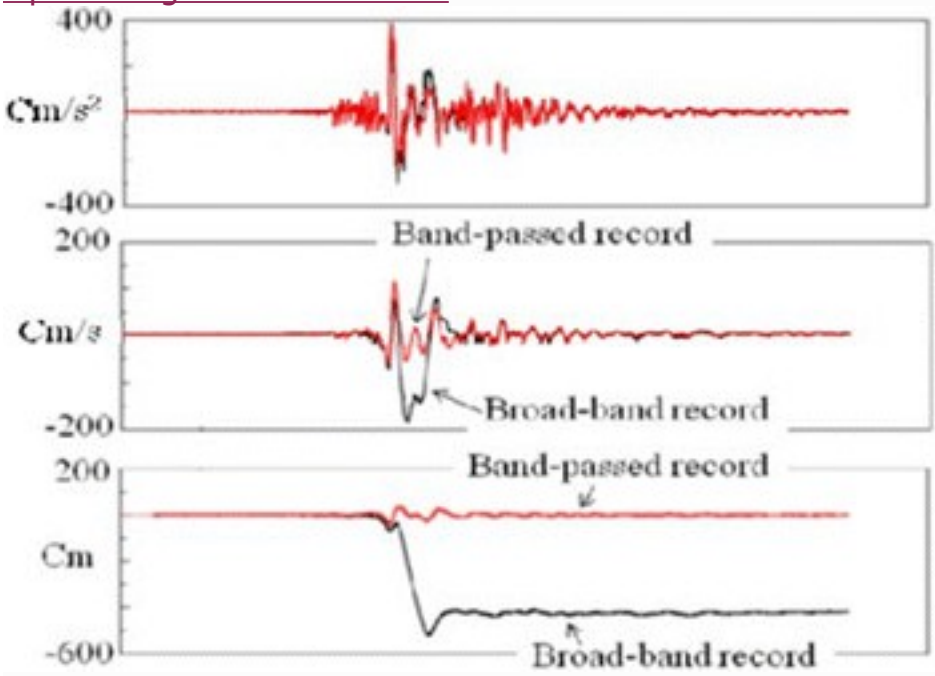

Fig. 18
Synthesized seismograms that would have caused damage (*black*). Filtered records (*red*)
McCallen et al. (2006) interpreted these records as a combination of the tectonic plate displacement moving north and a simultaneously arriving shear wave with first motion south. The result to the bridge was that due to

the long, 9 s natural period of the bridge, the movement of the roadway was delayed from the first arrival time of the fling pulse, and just as it was moving north, the shear wave arrived and pushed the bottom of the towers south. The resulting shear damaged road ties along the bridge (McCallen et al. 2006). Figure 19 shows very similar arrivals recorded from three recent earthquakes: M_w 7.5 1999 Taiwan, M_w 7.4 1999 Izmit, and M_w 7.3 1992 Landers earthquakes after reprocessing the records to recover long period motions (McCallen et al. 2006).

Open image in new window

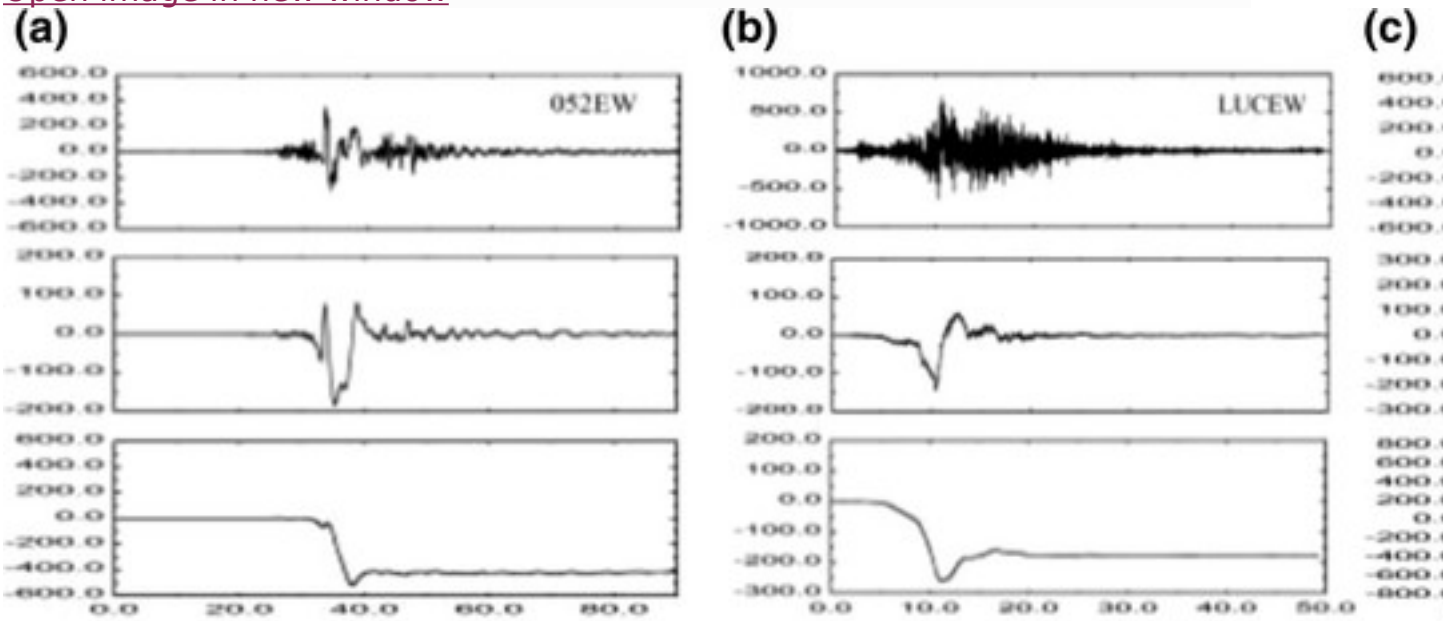

Fig. 19
Fault parallel fling and far-field shear wave; **a** 1999 Taiwan 052, **b** 1999 Turkey YPT, **c**Landers Lucerne

Another example of the need for a physical-based approach is the design of the new San Francisco–Oakland Bay Bridge, eastern span. Design response spectra are based upon regression of existing records, with regression modified to account for the fault rupture directivity effect. This would be roughly parallel to the length of the span (Fugro-Earth 2001). Furthermore, spectrum-compatible time histories used for dynamic analysis were developed with particular attention to the fault-normal directivity effect. While this is important, there is no provision in the design spectra or ground motions for the arrival of the far-field shear wave soon after the fault parallel near-field fling (Fig. 19). Finally, this type of ground motion has not been addressed by conventional methods because the traditional filtering of strong motion records eliminates the near-field portion of the records (Fig. 19).

9 Discussion and Conclusions

Making accurate earthquake hazard predictions requires a physical model for earthquakes and one approach is to use kinematic source models that are consistent with dynamic rupture, as we have discussed above, to generate rupture scenarios that span the variability of potential ground motion in a predictive situation. Fifty years of strong motion records are insufficient to capture all possible ranges of site and propagation path conditions, rupture processes, and spatial geometric relationships between source and site. Predicting future earthquake scenarios is necessary; models that have little or no physical basis but have been tested and adjusted to fit available observations can only “predict” what happened in the past, which is a form of description as opposed to true prediction. The ultimate solution for modeling earthquakes would be dynamic solutions that satisfy both elastodynamic equations and fracture mechanics, and that have known elastic constants and constituent relations for faulting processes. Estimates of these parameters for the fault zone carry large uncertainties and require several poorly bounded assumptions. The resultant uncertainties in computations limit their usefulness in better understanding of the earthquake process and in providing bounds for kinematic rupture models.

The basic premises of our source modeling for the purposes of ground-motion prediction are:

1. 1.
Accurate synthesis of recorded ground motions for a particular fault rupture scenario, sufficient for engineering purposes, is possible.
2. 2.
A general description of the rupture is sufficient for synthesizing realistic ground motions.
3. 3.
The rupture characteristics of a fault can be constrained in advance by interpreting physical properties such as geologic structure, seismicity, and regional tectonics.
4. 4.
The range of possible fault rupture scenarios is narrow enough to functionally constrain the range of strong ground motion predictions.
5. 5.
A discrete set of rupture scenarios is sufficient, for engineering purposes, to span the infinite combinations possible from a given range of rupture parameters.

An important corollary for testing this approach is that if a scenario earthquake matches the seismograms from an actual earthquake, then the rupture parameters of that scenario are comparable to what actually happened.

Both earthquake source models and ground-motion attenuation relationships are subject to significant uncertainties, which are expressed as probability distributions (giving an estimate of the median and standard deviation) of earthquake occurrence rates and ground motion relationships. The uncertainty in a ground motion relationship arises from the variability in source characteristics among events of the same size in the strong motion database and from the different earth structures through which seismic waves from events propagated. In PSHA studies, this is considered aleatory uncertainty, or the uncertainty due to inherent randomness of the process. Current PSHA studies are based upon the ergodic assumption that the randomness in space from several sources is the same as the randomness in time from the same source (Anderson and Brune 2000). With this ergodic assumption, correlation between the ground motion and the specific source, path, and site is lost, thereby leading to potentially higher total uncertainty in hazard estimates than if each earthquake source release of energy was individually propagated to the site of interest. There is also an attempt to model epistemic uncertainty, the uncertainty in knowledge about earthquake processes. This refers to factors such as strike, dip, and slip vector that could further reduce aleatory uncertainty if they were known and included as regression parameters.

Alternatively, a deterministic approach identifies significant faults or source zones and establishes the Maximum Possible Earthquake (MPE) for the Design Basis Earthquake (DBE). Deterministic hazard studies have had a problem identifying the appropriate source for each earthquake and their likelihood of occurrence and PSHA has had problems with insufficient historical data and accurately accounting for epistemic uncertainty with respect to the source and propagation of strong ground motion.

We can incorporate the combination of deterministic studies by calculating the actual earthquake rupture and recorded ground motion relevant to a particular site, and incorporating this into PSHA studies by replacing the use of attenuation relations. The output from this PSHA approach is a library of source- and site-specific ground-motion time series that would comprise a sample of all the earthquakes that could affect a site during its design life. The uncertainty of the PSHA is defined by bounds on the physical parameters that go into the computation of ground motion rather than having an unbounded PSHA developed from unbound shapes to probability distributions. Hutchings et al. (2007) showed that a realistic distribution of rupture parameters results in a bounded distribution of possible ground motion parameters and functionally constrains the range of strong ground motion predictions. The library of seismograms is used to either develop hazard curves of traditional engineering parameters, in the form of the annual probability of exceedance, or used directly in developing risk estimates. Current computational power and structural dynamic codes are

such that it is now possible to calculate risk directly from Gap Workshop Report (2012).

In many situations a critical facility is located in a seismically active area. Using the actual Green's functions for strong ground motion synthesis seems to be preferred to synthetic Green's functions. We have shown in several research papers (discussed in this manuscript) that the site conditions dominate the complexity of Green's functions and they do not have to be located exactly at the source location of the large event or have the same focal mechanism to significantly reduce the uncertainty in synthetic calculations. Further, the method discussed here uses many small earthquakes as the source of Green's functions. This averages out random errors when using EGFs. In addition, these circulations are for the linear site response. Soils engineers have to use this information to modify the calculations for non-linear site response (Heuze et al. 1997).

We have presented several validations for the source model and applied a strict test of how well synthesized seismograms fit observed records for engineering purposes using the Anderson test (Anderson 2004). Most of these validations are in the near-source region. It is this region that is most challenging to provide good syntheses for ground motions. Many studies have been satisfied that they have matched the ω-squared model, but are in the far field and non-physical. In fact (and for ours too), it is easy to match the ω-squared model in the far field in as long as the source model has a fractal distribution ($D = 2$) of high frequency (Frankel 1991). It is in near-source region, where the ω-squared model breaks down, where the source models are challenged. We have shown that using source parameters in solving the representation relation we match the ω-squared model in the far-field and the near-source area of many previous earthquakes. This is independent of scaling relation or target spectra. In applying the approach to PSHA, other rupture parameters that have not been previously observed in nature can also be applied to address extreme ground motions that have not been previously observed.

Notes

Acknowledgements

We benefited from technical editing by Mariel Nelson. Research was funded independently by the institutions listed as the authors' address.

References

1. Aagaard, B., Kientz, S., Knepley, M., Strand, L., & Williams, C. (2013). *PyLith user manual, version 2.0.0*. Davis, CA: Computational Infrastructure of Geodynamics.Google Scholar

2. Abrahamson, N. A., & Bolt, B. A. (1987). Array analysis and synthesis mapping of strong ground motion. In B.A. Bolt (Ed.), *Strong Motion Synthetics* (pp. 55–90). Orlando, Florida, U.S.A.: Academic Press.Google Scholar

3. Abrahamson, N. A., & Bommer, J. J. (2009). Sigma: Issues, insights, and challenges. *Seismological Research Letters, 80,* 41–56.Google Scholar

4. Aki, K., & Richards, P. G. (2002). Quantitative seismology (2nd ed.). University Science Books, ISBN: ISBN0935702962, 9780935702965, Sausalito, California, USA.Google Scholar

5. Anderson, J. G. (2004). A criterion for evaluating goodness of fit of accelerograms. In *13th World Conference on Earthquake Engineering*, Vancouver, B.C., Canada, August 1–6, paper No. 243.Google Scholar

6. Anderson, J. G., & Brune, J. (2000). Probabilistic seismic hazard analysis without the ergodic assumption. *Seismological Research Letters, 71,* 19–28.Google Scholar

7. Andrews, D. J., Hanks, T. C., & Whitney, J. W. (2007). Physical limits on ground motion at Yucca Mountain. *Bulletin of the Seismological Society of America, 97,* 1771–1792.CrossRefGoogle Scholar

8. Atkinson, G., & Macias, M. (2009). Predicted ground motions for great interface earthquakes in the Cascadia subduction zone. *Bulletin of the Seismological Society of America, 99,* 1552–1578.CrossRefGoogle Scholar

9. Baker, J. W., & Cornell, C. A. (2004). Uncertainity propagation in probabilistic seismic loss estimation. *Structural Safety, 30,* 236–252.CrossRefGoogle Scholar

10. Boatwright, J.L. (1981). Quasi-dynamic models of simple earthquake: an application to an aftershock of the 1975 Oroville, California earthquake. *Bulletin of the Seismological Society of America*, *71*, 69–94.Google Scholar

11. Boatwright, J., Fletcher, J. B., & Fumal, T. E. (1991). A general inversion scheme for source, site, and propagation characteristics using multiply recorded sets of moderate-sized earthquakes. *Bulletin of the Seismological Society of America, 81,* 1754–1782.Google Scholar

12. Bommer, Julian J., & Abrahamson, Norman A. (2006). Why do modern probabilistic seismic-hazard analyses often lead to increased hazard estimates? *Bulletin of the Seismological Society of America, 96,* 1967–

1977. doi: 10.1785/0120060043. **(Review Article)**.CrossRefGoogle Scholar

13. Boore, David M., Joyner, William B., & Fumal, Thomas E. (1997). Equations for estimating horizontal response spectra and peak acceleration from Western North American earthquakes: A summary of recent work. *Seismological Research Letters, 68,* 128–153.CrossRefGoogle Scholar

14. Campbell, K. W., & Bozorgnia, Y. (2003). Erratum: Updated near-source ground-motion (attenuation) relations for horizontal and vertical components of peak ground accelerations and aceleration response spectra. *Bulletin of the Seismological Society of America*, *93*, 1413.Google Scholar

15. Conte, J. P., Pandit, H., Stewart, J. P., & Wallace, J. W. (2003). Ground motion intensity measures for performance-based earthquake engineering. In: *Proceedings of the Ninth International Conference on Applications of Statistics and Probability in Civil Engineering (ICASP9), July 6–9*. San Francisco, USA.Google Scholar

16. Cornell, C. A. (1968). Engineering seismic risk analysis. *Bulletin of the Seismological Society of America, 58,* 1583–1606.Google Scholar

17. Das, S., & Kostrov, B. V. (1990). Inversion for seismic slip rate history and distribution with stabilizing constraints: Application to the 1986 Andreanof islands earthquakes. *Journal of Geophysical Research, 95,* 6899–6913. doi: 10.1029/90JB00701. **(ISSN: 0148-0227)**.CrossRefGoogle Scholar

18. Fenves, G. L., & Ellery, M. (1998). Behavior and failure analysis of a multiple-frame highway bridge in the 1994 Northridge Earthquake, Pacific Earthquake Engineering Research Center. Report No. PEER 98/08.Google Scholar

19. Fergany, E., & Hutchiings, L. (2017). Demonstration of pb-PSHA with Ras-Elhekma earthquake, Egypt. *NRIAG Journal of Astronomy and Geophysics* (in press, available online).Google Scholar

20. Foxall, B., Hutchings, L. J., & Kasameyer, P. W. (1996). Prediction of strong ground motion based upon physical constraints on fault rupture scenarios for ground motion prediction, Lawrence Livermore National Laboratory, UCRL-JC-11637.Google Scholar

21. Frankel, A. (1991). High-frequency spectral falloff of earthquakes, fractal dimension of complex rupture, b value, and the scaling of

strength on faults. *Journal of Geophysical Research, 96,* 6291–6302.CrossRefGoogle Scholar

22. Fugro-Earth Mechanics. (2001). Caltrans Seismic Advisory Board.Google Scholar

23. Gap Workshop Report. (2012). “Nuclear energy advancing modeling and systems campaign (NEAMS)”; conveners: James A. Blink (Lawrence Livermore National Laboratory) and Robert J. Budnitz (Lawrence Berkeley National Laboratory), March 15, 2012.Google Scholar

24. Golara, A., & Ahmady Jazany, R. (2013). An improvement on the use of empirical green functions for ground motion synthesis to predict Tehran’s main earthquake. *Scientific Research and Essays, 8*(19), 731–753.Google Scholar

25. Golara, A., & Hamzehloo, H. (2006). *Strong ground motion modeling for the 2004 Firozabad–Kojoor Earthquake, North of Iran*. First European Conference on Earthquake Engineering and Seismology (a joint event of the 13th ECEE and 30th General Assembly of the ESC) Geneva, Switzerland, 3–8 September. Paper Number: 895.Google Scholar

26. Graves, R. W., & Pitarka, A. (2010). Broadband ground-motion simulation using a hybrid approach. *Bulletin of the Seismological Society of America, 100,* 2095–2123.CrossRefGoogle Scholar

27. Guatteri, M. P., Mai, M., Beroza, G. C., & Boatwright, J. (2003). Strong ground-motion prediction from stochastic-dynamic source models. *Bulletin of the Seismological Society of America, 93,* 301–313.CrossRefGoogle Scholar

28. Guo-Quan, W., Zhou, X.-Y., Ma, Z.-J., & Zhang, P.-Z. (2001) A preliminary study on the randomness of response spectra of the 1999 Chi-Chi, Taiwan, earthquake. *Bulletin of the Seismological Society of America*, *91*, 1388–1389.Google Scholar

29. Hartzell, S. H. (1978). Earthquake aftershocks as Green’s functions. *Geophysical Research Letters*, *5*(1):1–4Google Scholar

30. Hartzell, S., Harmsen, S., Frankel, A. & Larsen, S. (1999). Calculation of broadband time histories of ground motion: comparison of methods and validation using strong-ground motion from the 1994 Northridge earthquake. *Bulletin of the Seismological Society of America*, *89*, 1484–1504.Google Scholar

31. Heuze, F. E., Ueng, T. S., Hutchings, L. J., Jarpe, S. P., & Kasameyer, P. W. (1997). A coupled seismic-geotechnical approach to site-specific

strong motion. *Soil Dynamic and Earthquake Engineering, 16*(4), 259–272.CrossRefGoogle Scholar

32. Hutchings, L. (1991). 'Prediction' of strong ground motion for the 1989 Loma Prieta earthquake using empirical Green's functions. *Bulletin of the Seismological Society of America, 81,* 88–121.Google Scholar

33. Hutchings, L. (1994). Kinematic earthquake models and synthesized ground motion using empirical Green's functions. *Bulletin of the Seismological Society of America, 84,* 1028–1050.Google Scholar

34. Hutchings, L., & Viegas G. (2012). *Application of Empirical green's functions in earthquake source, wave propagation and strong ground motion studies*. Earthquake Research and Analysis, New Frontiers in Seismology, chapter 3, 87-140. Edited by Sebastiano D'Amico, InTech Publishing, on-line link: http://www.intechopen.com/search?q=New+Frontiers+in+Seismology.

35. Hutchings, L., Foxall, B., Kasameyer, P., Larsen, S., Hayek, C., Tyler-Turpin, C., Aquilino, J., & Long, L. (2005*). Deep borehole instrumentation along San Francisco bay bridges: 1996–2003 and strong ground motion synthesis along the San Francisco/Oakland Bay Bridge*. Final Report, Lawrence Livermore National Laboratory, Livermore, CA, UCRL-TR-2117303.Google Scholar

36. Hutchings, L., Ioannidou, E., Jarpe, S., & Stavrakakis, G. N. (1997). *Strong ground motion synthesis for a M = 7.2 earthquake in the Gulf of Corinth, Greece using empirical Green's functions*. Lawrence Livermore National Laboratory, Livermore, CA, UCRL-JC-129394.Google Scholar

37. Hutchings, Lawrence, Ioannidou, Eleni, Kalogeras, Ioannis, Voulgaris, Nicholas, Savy, Jean, Foxall, William, et al. (2007). A physically based strong ground-motion prediction methodology; Application to PSHA and the 1999 M=6.0 Athens Earthquake. *Geophysical Journal International, 168,* 569–680.CrossRefGoogle Scholar

38. Hutchings, L., & Jarpe, S. (1996). Ground-motion variability at the highway 14 and I-5 interchange in the Northern San Fernando valley. *Bulletin of the Seismological Society of America, 86,* S289–S299.Google Scholar

39. Hutchings, L., Jarpe, S., & Kasameyer, P. (1998). *Validation of a ground motion synthesis and prediction methodology for the 1988, M = 6.0, Saguenay Earthquake*. Lawrence Livermore National Laboratory, Livermore, CA, UCRL-JC-129395.Google Scholar

40. Hutchings, L. J., Jarpe, S. P., Kasameyer, P. W., & Foxall, W. (1996). *Synthetic strong ground motions for engineering design utilizing empirical Green's functions*. Presented at Eleventh World Conference of Earthquake Engineering, Acapulco, June 23–28, 1996 (CDROM Elsevier); available from Lawrence Livermore National Laboratory, Livermore, CA, UCRL-JC-123762.Google Scholar

41. Hutchings, L., Kasameyer, P. W., & Foxall, W. (2003). *LLNL* (p. 135697). Lawrence Livermore National Laboratory, Livermore, CA, UCRL-ID: Hazard mitigation center ground motion prediction methodology.Google Scholar

42. Hutchings, L., & Wu, F. (1990). Emprical green's functions from small earthquakes: A waveform study of locally recorded aftershocks of the 1971 San Fernando earthquake. *Journal of Geophysical Research, 95,* 1187–1214.CrossRefGoogle Scholar

43. IAEA. (2007). *IAEA Issues report on Kashiwazaki–Kariwa nuclear plant*. https://www.iaea.org/newscenter/news/iaea-issues-report-kashiwazaki-kariwa-nuclear-plant.

44. IAEA. (2014). *Nuclear power plants and earthquakes*. http://www.world-nuclear.org/information-library/hsafety-and-security/safety-of-plants/nuclear-power-plants-and-earthquakes.aspx.

45. Ioannidou, E., Voulgaris, N., Kalogeras, N., Hutchings, I., & Stavrakakis, G. (2001). Analysis of site response in the Athens area from the 7 September 1999, Mw = 5.9 Athens earthquake and aftershock recordings, and intensity observations. Bollettino di Geofisica Teorica ed Applicata, Special Issue on Site Response, December 2001.Google Scholar

46. Irikura, K. (1986). Prediction of strong acceleration motion using empirical Green's function. Proc. 7th Japan Earthq. Eng. Synp. 151-156.Google Scholar

47. Jarpe, S., & Kasameyer, P. K. (1996). Validation of a methodology for predicting broadband strong motion time histories using kinematic rupture models and empirical Green's functions. *Bulletin of the Seismological Society of America, 86,* 1116–1129.Google Scholar

48. Joyner, W. B., & Boore, D. M. (1986). On simulating large earthquakes by green's-function addition of smaller earthquakes. In S. Das, J. Boatwright, & C. H. Scholz (Eds.) *Earthquake Source Mechanics, Geophysical Monograph 37 Maurice Ewing*, vol. 6 (pp. 269-274). Washington, DC, USA: American Geophysical Union.Google Scholar

49. Kiratzi, A., Karakaisis, G., Papadimitriou, E., & Papazachos, B. (1985). Seismic source-parameter relations for earthquakes in Greece. *Pure and Applied Geophysics, 123,* 27–41.CrossRefGoogle Scholar

50. Larsen, S., & Schultz, C. A. (1995). *ELAS3D: 2D/3D elastic finite-difference wave propagation code, Technical Report UCRL-MA-121792*. Livermore: Lawrence Livermore National Laboratory.Google Scholar

51. Liu, P., Custódio, S., & Archuleta, R. J. (2006). Kinematic inversion of the 2004 Mw6.0 Parkfield earthquake including site effects. *Bulletin of the Seismological Society of America, 96,* S143–S158.CrossRefGoogle Scholar

52. Makris, J., Papoulia, J., & Drakatos, G. (2004a). Tectonic deformation and microseismicity of the Saronikos Gulf, Central Greece. *Bulletin of the Seismological Society of America, 94,* 920–929.CrossRefGoogle Scholar

53. Makris, J., Papoulia, J., Ilinski, D., & Karastathis, V. (2004a). *Crustal study of the Saronikos–Corinthiakos basins from wide aperture seismic data: Intense crustal thinning below the Saronikos Basin*. 10th Conference of the Hellenic Geological Society, Thessaloniki, Greece (**Abstract**).Google Scholar

54. McCallen, D. B., & Hutchings, L. J. (1996). Ground motion estimation and nonlinear seismic analysis. LLNL, UCRL-JC-121667. In: *Proceedings of the 12th Conference on Analysis and Computation of the American Society of Civil Engineers*. Chicago, Illinois.Google Scholar

55. McCallen, D., Astaneh-Asl, A., Larsen, S., & Hutchings, L. (2006). *Dynamic response of the suspension spans of the San Francisco-Oaklnad Bay Bridge*. Proceedings of the 8th US National Conference on Earthquake Engineering April 18-22, San Francisco, California, USA, Paper No. 952.Google Scholar

56. McCallen, D. B., Astaneh-Asl, A., Larsen, S. C. (2015). Near-field earthquake ground motions and the response of building structures. Report no 2273, global security computing applications division (p. 57). Lawrence Livermore National Laboratory, Livermore, CA.Google Scholar

57. Mert A., Fahjan, Y., & Hutchings, L. (2010). Prens adaları fayındaki depremlerin kaynak parametrelerinin eş zamanlı ve tekil ters çözüm teknikleri ile belirlenmesi. İstanbul Yerbilimleri Dergisi, C.23, S.1, SS. 53,63.Google Scholar

58. Mert, A., Fahjan, Y., Pinar A., & Hutchings, L. (2014). Earthquake simulation studies for the Marmara region using empirical Green's functions method (**submitted**).Google Scholar

59. Mert, A., Fahjan, Y., Pınar, A., & Hutchings, L. (2011). *İstanbul için tasarım esaslı kuvvetli yer hareketi dalga formlarının zaman ortamında türetilmesi. 1. Türkiye Deprem Mühendisliği ve Sismoloji Konferansı, ODTÜ, Ankara*. http://search.mymapsxp.com/?uid=f21c2878-56f54c1a96ca49ded5451765&uc=20150713&source=pd_gs_g_map_mapquest_directions&page=homepage&implementation_id=Maps_xp_0.0.2L .

60. Mert, A., Fahjan, Y., Pınar, A., & Hutchings, L. (2012). *EGF simulation of high frequency ground motion. A case study for Mw = 5.0 Central Marmara Fault Earthquake*, 15 WCEE, Lisbon.Google Scholar

61. Miah, M. (2016). *Development of a dynamic coupled hydro-geomechanical code and its application to induced seismicity*. Dissertation, Department of Civil Engineering, The University of Mississippi.Google Scholar

62. NISA. (2008). KashiwZAKI-kARIWA Nuclear Power Station, Tokoyo Electric Power Company. Interim Report on the Geology and Geological Structure of the Ground Surrounding the Site and on the Evaluation of the Design Basis Ground Motion, Nuclear and Industrial Safety Agency, November 18.Google Scholar

63. Orowan, E. (1960). Mechanism of seismic faulting. *Geological Society of America Bulletin,79,* 323–345.CrossRefGoogle Scholar

64. Papanikolaou, D., Lykousis, V., Chronis, G., & Pavlakis, P. (1988). A comparative study of Neotectonic basins along the Hellenic Arc: The Messiniakos, Argolikos, Saronikos and Southern Evoikos Gulf. *Basin Research, 1,* 167–176.CrossRefGoogle Scholar

65. Papoulia, J., Fahjan, Y.M., Hutchings, L., & Novikova, T. (2015). PSHA for broad-band strong ground-motion hazards in the Saronikos Gulf, Greece, from potential earthquake with synthetic ground motions. *Journal of Earthquake Engineering,* 624–648. doi: 10.1080/13632469.2014.991977.

66. Pavic, R., Koller, M. G., Bard, P.-Y., & Lacave-Lachet, C. (2000). Ground Motion prediction with the empirical Green's function technique: an assessment of uncertainties and confidence level. *Journal of Seismology*, *4*, 59–77.Google Scholar

67. Porter, K. A. (2003). *An overview of PEER's performance-based earthquake engineering methodology*. Department of Civil Engineering, California Institute of Technology, Pasadena, CA.Google Scholar

68. Schulz, C. H. (2002). *The mechanics of earthquakes and faulting* (p. 471). Cambridge: Cambridge University Press.Google Scholar

69. Scognamiglio, Laura, & Hutchings, Lawerence. (2009). A test of a physically-based strong ground motion prediction methodology with the 27 September 1997, Mw = 6.0 Colfiorito Earthquake (Umbria-Marcha Sequence), Italy Earthquake. *Tectonophysics, 476,* 145–158.CrossRefGoogle Scholar

70. Senior Seismic Hazard Analysis Committee (SSHAC), Budnitz, R. J., Apostolakis, G., Boore, D. M., Cluff, L. S., Coppersmith, IC J., Cornell, C. A., & Morris, P. A. (1997). Recommendations for probabilistic seismic hazard analysis: guidance on uncertainty and use of experts. NUREG/CR-6372, Lawrence Livermore National Laboratory, UCRL-ID-122160. V1.Google Scholar

71. Somerville, P. G., Sen, M., & Cohee, B. (1991). Simulation of strong ground motion recorded during the 1985 Michoacan Mexico and Valparaiso, Chile earthquakes. *Bulletin of the Seismological Society of America*, *81*, 1–28.Google Scholar

72. Somerville, P., Irikura, K., Graves, R., Sawada, S., Wald, D., Abrahamson, N., et al. (1999). Characterizing crustal earthquake slip models for the prediction of strong ground motion. *Seismological Research Letters, 70,* 59–80.CrossRefGoogle Scholar

73. Stepp, J. S., & Wong, I. G. (2003). Probabilistic seismic hazard analysis for Yucca Mountain. In *Presentation to the Nuclear Waste Technical Review Board*, February 24, 2003.Google Scholar

74. Strasser, F. O., Abrahamson, N. A., & Bommer J. J. (2009). Sigma: Issues, insights, and challenges. *Seismological Research Letters, 80*.Google Scholar

75. Tse, S. T., & Rice, J. R. (1986). Crustal earthquake instability in relation to the depth variation of frictional slip properties. *Journal of Geophysical Research, 91,* 9452–9472.CrossRefGoogle Scholar

76. Tullis, T. E., Richards, K., Barall, M., Dieterich, J. H., Field, E. H., Hein, E. M., et al. (2012). Comparrison among observations and earthquake simulator results for the allcal2 california fault model. *Bulletin of the Seismological Society of America, 83,* 994–1006.Google Scholar

77. Tumarkin, A. (1994). Energy constraints on synthesis of strong ground motion, Abs. *American Geophysical Union, San Francisco, 4,* 59–77.Google Scholar

78. Uetake, T., Nishimura, I., & Mizutani, H. (2008). *Characteristics of strong motion records in Kashiwazaki–Kariwa nuclear power station during the Niigataken Chuetsu–Oki earthquake in 2007*. The 14 World

Conference on Earthquake Engineering October 12–17, 2008, Beijing, China.Google Scholar

79. USNRC. (1980). *Reconnaissance report: Effects of November 8, 1980 earthquake on Humboldt Bsy Power Plant and Eureka*. California area, U.S. Nuclear Regulatory Commission (pp. 1–8).Google Scholar

80. Wang, S. (2006). Understanding seismic hazard and risk assessments: an example in the new madrid seismic zone of the central United States. Proceedings of the 8th U.S. National Conference on Earthquake Engineering April 18–22, 2006, San Francisco, California, USA, Paper No. 416.Google Scholar

81. Wells, D. L., & Coppersmith, K. J. (1994). New empirical relationships among magnitude, rupture length, rupture width, rupture area, and surface displacement. *Bulletin of the Seismological Society of America, 84,* 974–1002.Google Scholar

82. Wollen, E., Seth, S., Pazzaglia, F., Meltzer, A., Kafka, A., & Berti, C. (2012). Mineral, Virginia, earthquake illustrates seismicity of a passive-aggressive margin. *Geoph Res Lett,39,* 2.Google Scholar

83. Wossner, J., Treml, M., & Wenzel, F. (2002). Simulation of Mw = 6.0 earthquakes in the Upper Rhinegraben using Empirical Green functions. *Geophysical Journal International,151,* 487–500.CrossRefGoogle Scholar

84. Wu, F. T. (1978). Prediction of strong ground motion using small earthquakes. Proceedings of 2nd International Conference on Microzonation National Science Foundation, San Francisco, CA, pp. 701–704.Google Scholar